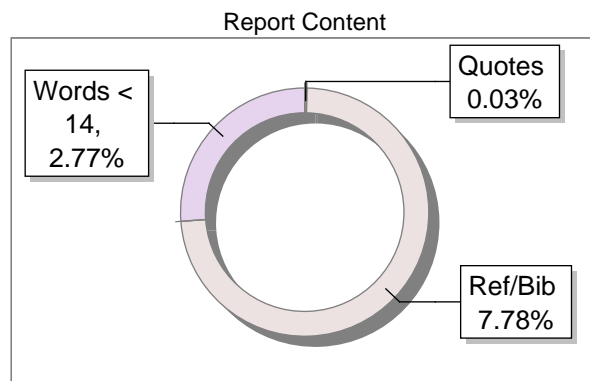
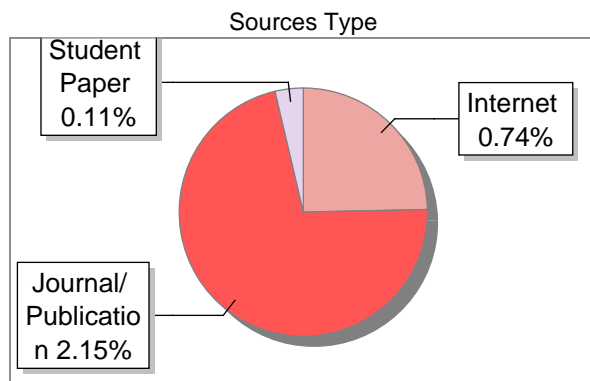


Submission Information

Author Name	Nsenga Ngoie Idriss
Title	Non-Invasive Intracranial Monitoring Using EEG Signals for Epilepsy
Paper/Submission ID	4834430
Submitted by	asklibrarian@acharya.ac.in
Submission Date	2025-12-08 12:49:21
Total Pages, Total Words	118, 18293
Document type	Project Work

Result Information

Similarity **3 %**



Exclude Information

Quotes	Excluded
References/Bibliography	Excluded
Source: Excluded < 14 Words	Not Excluded
Excluded Source	0 %
Excluded Phrases	Not Excluded

Database Selection

Language	English
Student Papers	Yes
Journals & publishers	Yes
Internet or Web	Yes
Institution Repository	Yes

A Unique QR Code use to View/Download/Share Pdf File





DrillBit Similarity Report

3

SIMILARITY %

55

MATCHED SOURCES

A

GRADE

- A-Satisfactory (0-10%)
- B-Upgrade (11-40%)
- C-Poor (41-60%)
- D-Unacceptable (61-100%)

LOCATION	MATCHED DOMAIN	%	SOURCE TYPE
2	IEEE 2020 International Conference on Artificial Intelligence and Signal Proce by Gupta-2020	<1	Publication
5	arxiv.org	<1	Publication
6	arxiv.org	<1	Publication
8	akademiabaru.com	<1	Publication
9	ieeexplore.ieee.org	<1	Publication
10	arxiv.org	<1	Publication
11	devicematerialscommunity.nature.com	<1	Internet Data
12	Real-Time Epileptic Seizure Detection Using EEG by Vidyaratne-2017	<1	Publication
13	Paper Published in International Journal of Materials - MDPI 2015	<1	Student Paper
14	thesai.org	<1	Publication
15	www.hindawi.com	<1	Internet Data
16	www.intechopen.com	<1	Publication
17	www.mdpi.com	<1	Internet Data
18	escholarship.org	<1	Internet Data

- 19** Studies on crystallization process for pharmaceutical compounds using ANN modeling and model based, by Reddy, P. Swapna, Yr-2023 <1 Publication
- 21** www.linkedin.com <1 Internet Data
- 22** An over-the-horizon potential safety threat vehicle identification method based on ETC big data, by Luo, Guanghao, Yr-2023 <1 Publication
- 23** arxiv.org <1 Publication
- 24** A holistic motility understanding of the social phenomena underlying inter-city, by Lin, Siyi, Yr-2024 <1 Publication
- 25** frontiersin.org <1 Internet Data
- 26** Integrated horizontal convective PCR system for clinical diagnostics By Wenshang Guo, Minghui Xu, Ye, Yr-2025,8,8 <1 Publication
- 27** Loss of the Low-Frequency Component of the Global-Flash Multifocal Electroretino by Luo-2011 <1 Publication
- 28** SNA Networks of Small Systems by Baratz-1985 <1 Publication
- 29** www.dx.doi.org <1 Publication
- 30** www.mdpi.com <1 Internet Data
- 31** www.sciencedirect.com <1 Internet Data
- 32** www.scribd.com <1 Internet Data
- 33** www.thinkmind.org <1 Publication
- 34** academicworks.cuny.edu <1 Internet Data
- 35** aircconline.com <1 Publication
- 36** Artificial intelligence and open science in discovery of disease-modifying medi, by Cheng, Feixiong, Yr-2024 <1 Publication

- 37** Artificial intelligence and open science in discovery of disease-modifying medi, by Cheng, Feixiong, Yr-2024 <1 Publication
- 38** arxiv.org <1 Publication
- 39** Biodegradation Natural and synthetic materials Edited by WB Betts Springer by Graha-1992 <1 Publication
- 40** cinc.org <1 Internet Data
- 42** Clinical large language model to predict loss to follow up for oncology patient By Tianshi Liu, Ziyi Chen, Yongh, Yr-2024,6 <1 Publication
- 44** Derivation Process of Vision That Bind the Overall Business Performance by Khiew-2017 <1 Publication
- 45** Detecting Landscape Disturbance at the Nasca Lines Using SAR Data Coll by Comer-2017 <1 Publication
- 46** docplayer.net <1 Internet Data
- 47** dspace.lib.cranfield.ac.uk <1 Publication
- 48** fdokumen.id <1 Internet Data
- 49** Femoral Fracture in Elderly An Avoidable Cause by Sartori-2018 <1 Publication
- 50** Impact of a Mass Media Vasectomy Promotion Campaign in Brazil by D- 1996 <1 Publication
- 51** juniperpublishers.com <1 Publication
- 52** mcet.in <1 Publication
- 53** Paper Published in International Journal of Materials - MDPI 2015 <1 Student Paper
- 54** Reliable Actual Fabric-Based Organic Light-Emitting Diodes Toward a Wearable Di by Kim-2016 <1 Publication

- 55** Scalp EEG Acquisition in a Low-Noise Environment A Quantitative Assessment by Zandi-2011 <1 Publication
-
- 56** Studying Within-Person Variation and Within-Person Couplings in Intensive Longit by Neubauer-2020 <1 Publication
-
- 57** thesai.org <1 Publication
-
- 59** www.ou.edu <1 Publication
-
- 60** www.theseus.fi <1 Publication
-
- 61** IEEE 2014 International Joint Conference on Neural Networks (IJCNN) <1 Publication by
-
- 62** IEEE 2018 IEEE Biomedical Circuits and Systems Conference (BioCAS) , by Burrello, Alessio - 2018 <1 Publication
-
- 63** IEEE 2019 29th International Conference on Field Programmable Logic <1 Publication
-

Abstract

Epilepsy is a chronic neurological disorder characterised by sudden, recurrent seizures caused by abnormal brain activity. This project presents a non-invasive EEG-based intracranial monitoring system designed to detect early seizure patterns using advanced DSP algorithms and machine-learning-driven feature extraction. The system integrates real-time data acquisition, noise filtering, spectral analysis, and classifier-based decision support to improve diagnostic accuracy and latency. A dual-microcontroller architecture optimises performance for STM32 for DSP computation and ESP8266 for visualisation, providing a low-cost, portable, and accessible solution suited for clinical and remote monitoring applications.

Keywords: Epilepsy, EEG, Seizure Detection, Digital Signal Processing, Feature Extraction, Machine Learning, Biomedical Monitoring, Low-Cost Healthcare.

Contents

1	Introduction	1
2	Literature Survey	7
3	Methodology and Working Principle	21
3.1	EEG Acquisition Method.....	22
3.2	Dataset Used for Model Training ³⁶	23
3.3	Signal Preprocessing and Noise Handling.....	25
3.4	Segmentation	26
3.5	Feature Extraction Overview	27
3.6	Classification Models	28
3.7	Embedded Deployment Strategy	28
3.8	Wireless Transmission and Alerting	29
3.9	Summary of Working Principle	29
4	Hardware Implementation	30
4.1	EEG Electrodes and Sensor Interface	31
4.2	BioAmp EXG Pill – Analog Front-End (AFE).....	32
4.3	STM32F446RE Microcontroller Unit.....	34
4.4	ESP-12E (ESP8266) Wireless Module	38
4.5	Local Alerting Mechanism	40
4.6	Power Supply and Regulation	41
4.7	Wiring Diagram and PCB Layout	42
4.8	Summary	44
5	Software Implementation	45
5.1	Firmware Execution Model	46
5.2	ADC Sampling and Preprocessing.....	47

5.3	Digital Signal Processing (DSP) Pipeline	48
5.3.1	50 Hz Notch Filter	48
5.3.2	301-Tap FIR Band-Pass Filter (0.5–45 Hz)	49
5.3.3	Sub-Band FIR Filtering	49
5.4	Windowing and Segmentation	50
5.5	Feature Extraction (24 Features)	51
5.5.1	Time-Domain Features	51
5.5.2	Hjorth Parameters	51
5.5.3	Frequency-Domain Features	52
5.5.4	Statistical Features	54
5.5.5	Nonlinear Features	56
5.5.6	MFCC-Like Features	58
5.5.7	AR Residual (Burg Method)	59
5.6	Machine Learning Model Development	62
5.7	CNN–LSTM Architecture (Used but slight lower Accuracy)	62
5.7.1	Random Forest Classifier (Higher Accuracy: 93.51%)	64
5.8	Embedded Seizure Detection Logic	65
5.9	Wireless JSON Transmission (ESP-12E)	65
5.10	ESP-12E Web Dashboard Firmware	66
5.11	Summary	72
6	Advantages	73
6.1	Non-Invasive, Safe, and Comfortable for Long-Term Use	73
6.2	Real-Time Seizure Detection With Low Latency	73
6.3	High Diagnostic Reliability Through DSP + ML Fusion	74
6.4	Low Power Consumption and Embedded Efficiency.....	75
6.5	Wireless Connectivity and Remote Health Monitoring	75
6.6	Cost-Effective Compared to Clinical EEG Systems	76

Non-Invasive Intracranial Monitoring Using EEG Signals for Epilepsy	2025–26
6.7 Modular, Extensible, and Research Friendly	76
6.8 Enhanced Patient Safety Through Immediate Alerts	77
6.9 Suitable for Home, Community, and Clinical Use.....	77
6.10 Summary of Advantages	78
7 Limitations	79
7.1 Limitations of Non-Invasive Scalp EEG.....	79
7.2 Analog Front-End (AFE) and Electrode Limitations.....	80
7.3 Hardware Constraints of STM32 Microcontroller	81
7.4 DSP and Feature Extraction Limitations	82
7.5 Machine Learning Limitations.....	83
7.6 Wireless Communication Constraints.....	85
7.7 Dataset and Model Generalizability Limitations	85
7.8 Clinical Validation Limitations.....	86
7.9 Summary	86
8 Applications	87
8.1 Clinical Epilepsy Monitoring	87
8.2 Home-Based Long-Term Epilepsy Management	87
8.3 Wearable IoT Health Devices	88
8.4 Seizure Alerting Systems to Reduce SUDEP Risk	88
8.5 Remote Patient Monitoring and Telemedicine	89
8.6 Mobile and Rural Healthcare Deployment	89
8.7 Academic, Engineering, and Research Applications	90
8.8 Data Acquisition for AI-Based Epilepsy Research	90
8.9 Educational Tool for DSP, Embedded Systems, and Neuroscience	91
8.10 Assistive Technology for Vulnerable Populations.....	91
8.11 Summary	91
9 Results and Discussion	92

9.1 Evaluation of DSP Filtering Pipeline.....	92
9.2 Feature Extraction Behaviour Across Classes.....	93
9.3 Machine Learning Performance (RF vs. CNN–LSTM)	95
9.4 PCA Clustering (2D and 3D).....	99
9.5 Embedded Real-Time Performance on STM32	100
10 Conclusion & Future Scope	102
10.1 Conclusion.....	102
10.2 Future Scope	103
10.3 Summary	106
APPENDIX	107
REFERENCES	108

1 Introduction

Epilepsy is a chronic neurological disorder characterised by recurrent, unprovoked seizures caused by abnormal, excessive electrical activity in the brain. According to the World Health Organization (WHO), nearly 18 million individuals worldwide are living with epilepsy, making it one of the most widespread neurological conditions [49]. The disorder is associated with significant social, psychological, and economic challenges, especially in low-resource regions where diagnostic and monitoring facilities are limited.

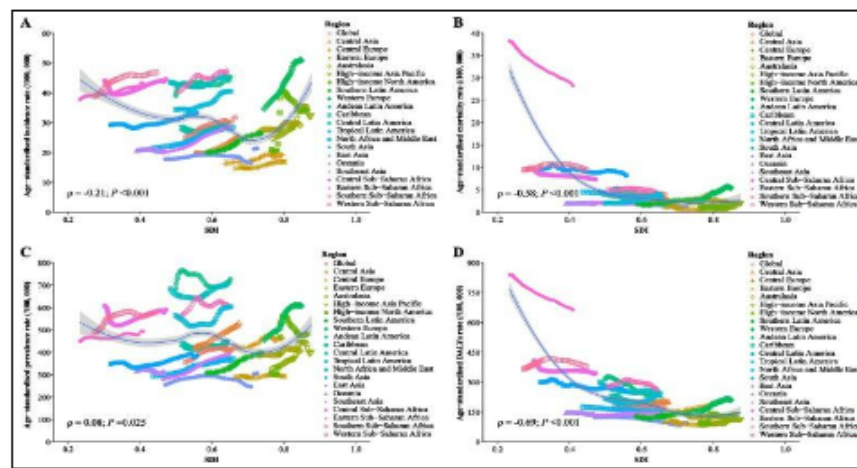


Figure 1: Global epilepsy distribution and prevalence statistics [51].

Seizures can vary widely—from focal seizures involving specific brain regions to generalised seizures that affect both hemispheres. These events generate distinct electrophysiological signatures observable through Electroencephalography (EEG), which remains the gold-standard non-invasive tool for identifying epileptiform activity [27]. Clinicians visually inspect EEG waveforms for hallmark patterns such as spikes, sharp waves, and spike-and-wave complexes.

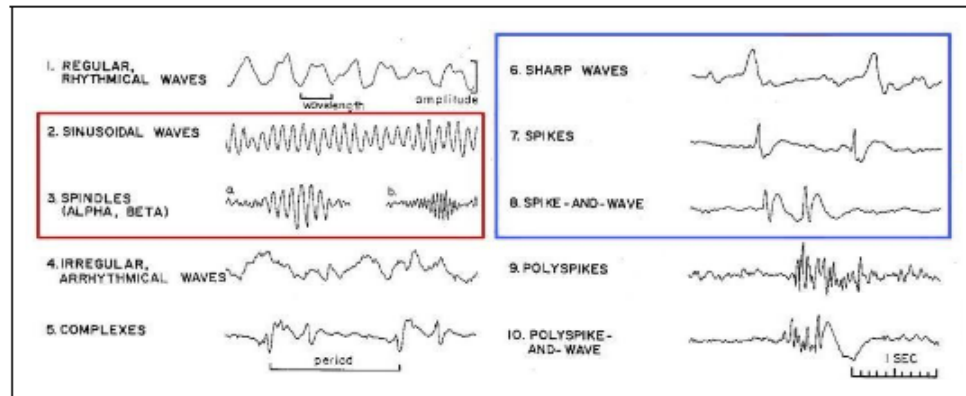


Figure 2: Typical EEG seizure waveforms (spike, sharp wave, spike-and-wave) [52].

Despite its diagnostic value, traditional EEG systems pose several limitations:

- They require clinical-grade amplifiers, shielded rooms, and controlled environments.
- Long-term EEG monitoring is costly and impractical outside hospitals.
- The equipment is bulky and restricts patient mobility.
- Continuous supervision by trained technicians is necessary.

These challenges hinder effective monitoring, particularly since many seizures occur unexpectedly outside clinical environments [36]. Portable, real-time EEG systems can bridge this gap by enabling continuous monitoring in homes, schools, workplaces, and rural health settings.

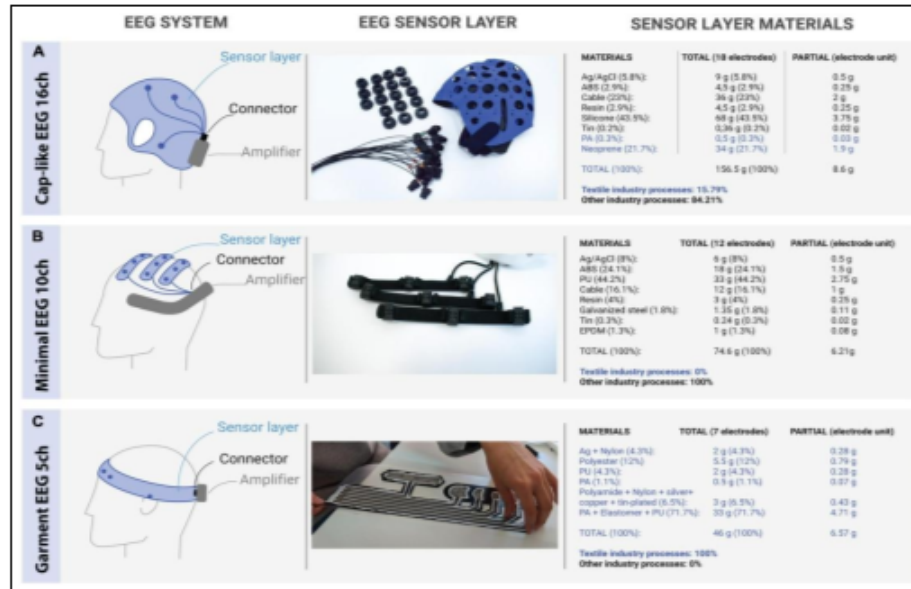


Figure 3: Comparison between traditional clinical EEG systems and wearable embedded EEG devices [25].

Background and Motivation

Epilepsy poses risks not only due to the seizures themselves but also due to complications such as injuries, falls, and Sudden Unexpected Death in Epilepsy (SUDEP). Continuous long-term monitoring significantly improves diagnostic yield; however, conventional EEG cannot provide practical round-the-clock observation [14]. The unpredictability of seizures amplifies the need for systems capable of real-time detection in everyday environments.

Recent advancements have made this possible. Research in biosignal acquisition has produced compact, low-noise analogue front ends (AFEs) capable of capturing microvolt-level EEG signals reliably outside laboratory conditions [9]. Concurrently, embedded processors like the STM32 enable real-time digital signal processing (DSP), and machine learning (ML) models provide automated seizure classification [2, 38].

Furthermore, IoT-enabled health systems allow wireless transmission of EEG-derived alerts to caregivers, dramatically improving patient safety [11]. These technological developments collectively motivate the design of a portable EEG monitoring system capable of real-time seizure detection.

Problem Statement

Although several EEG-based seizure detection systems exist, most face the following limitations:

- High cost and lack of portability.
- Noise sensitivity and reduced signal quality outside clinical settings.
- Absence of automated DSP and ML-based detection.
- Limited availability in rural healthcare infrastructure.
- Inability to perform real-time monitoring with low power consumption.

Thus, there is a clear need for a compact, affordable, embedded EEG system capable of continuous non-invasive monitoring and real-time seizure classification [43].

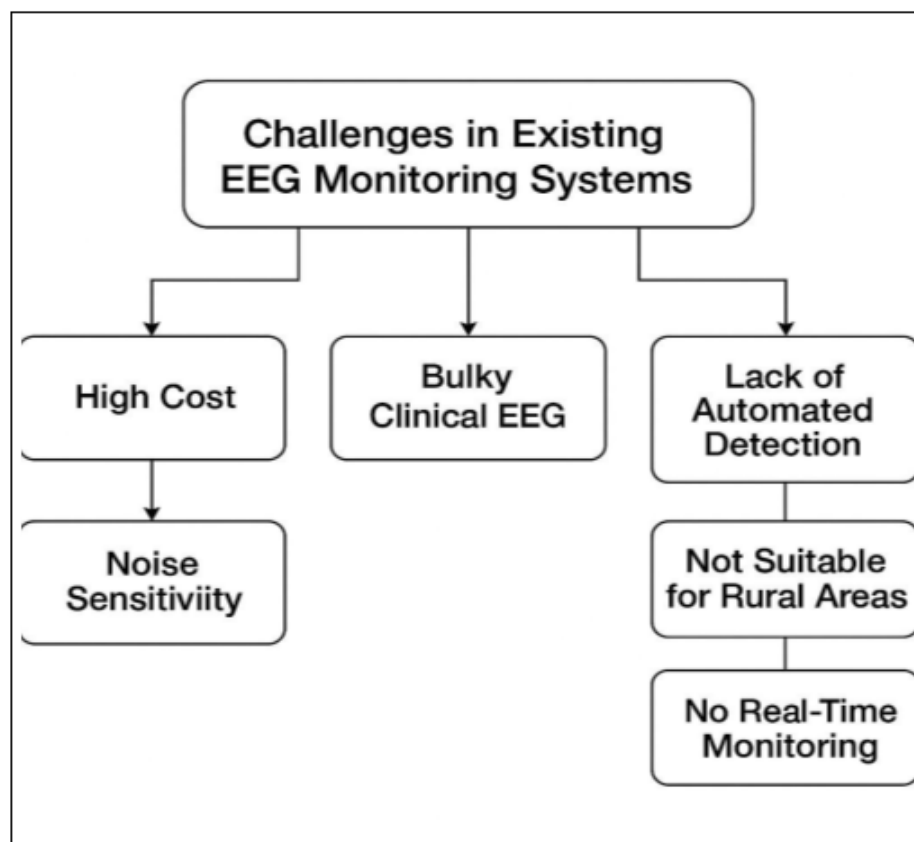


Figure 4: Key challenges in existing EEG monitoring systems.

Need for a Portable, Non-Invasive Monitoring System

Non-invasive EEG offers a safe and scalable method for long-term monitoring compared to intracranial EEG (iEEG), which requires surgical implantation and carries additional medical risks [13]. Recent advancements in embedded biosignal processing show that even single-channel or reduced-lead EEG can be effectively used for seizure detection when paired with ML and DSP pipelines [39].

The need for such a system is driven by:

- increased accessibility in rural and low-income regions,
- elimination of dependence on continuous hospital-based monitoring,
- real-time alerting for caregivers,
- lower operational and maintenance costs,
- improved diagnostic yield from long-term monitoring.

Scope of the Project

The project focuses on developing a complete end-to-end embedded seizure detection system incorporating:

- non-invasive EEG acquisition using the BioAmp EXG Pill,
- real-time DSP filtering, segmentation, and feature extraction,
- CNN–LSTM and Random Forest classification (both evaluated),
- on-device inference using optimised feature-based models,
- wireless transmission via ESP-12E,
- buzzer-based local alerts.

This scope ensures a functional, low-cost system ²⁶ suitable for both home use and clinical preliminary screening.

Objectives

The main objectives of this work are:

1. To develop a portable, single-channel EEG acquisition system.
2. To implement real-time DSP for noise reduction and signal enhancement.
3. To extract clinically relevant features for seizure classification.
4. To evaluate CNN–LSTM and Random Forest models (92.51% and 93.51% accuracy respectively).
5. To perform embedded inference on STM32 within strict time constraints.
6. To transmit real-time seizure alerts via ESP-12E.
7. To validate system performance against datasets collected from:
 - our own sensor-inactive recordings,
 - our own normal EEG recordings,
 - CHB-MIT + other online seizure datasets.

2 Literature Survey

Epileptic seizure detection has been widely studied across clinical neurology, biomedical engineering, digital signal processing (DSP), and artificial intelligence (AI). Over the past two decades, research has shifted from manual EEG interpretation to automated ML and deep

learning models, and more recently toward embedded, real-time, low-power seizure detection systems. This chapter reviews the state of the art, divided into three major domains:

1. Medical and clinical techniques for epilepsy diagnosis,
2. AI and DSP-based automated seizure detection approaches,
3. Deployment challenges, embedded implementations, and research gaps.

The structure and depth of coverage follow the style commonly used in EEG research papers and reflect the methodological framework adopted in this project.

A. Medical and Clinical Techniques

Electroencephalography (EEG) has been the cornerstone of epilepsy diagnosis for over 80 years. Traditional clinical EEG interpretation relies on neurologists visually identifying epileptiform discharges such as spikes, sharp waves, spike-and-wave complexes, and high-frequency bursts [27]. Noachtar et al. provided an authoritative description of EEG hallmark patterns used in epilepsy diagnosis, highlighting waveform morphology and spatiotemporal evolution [28].

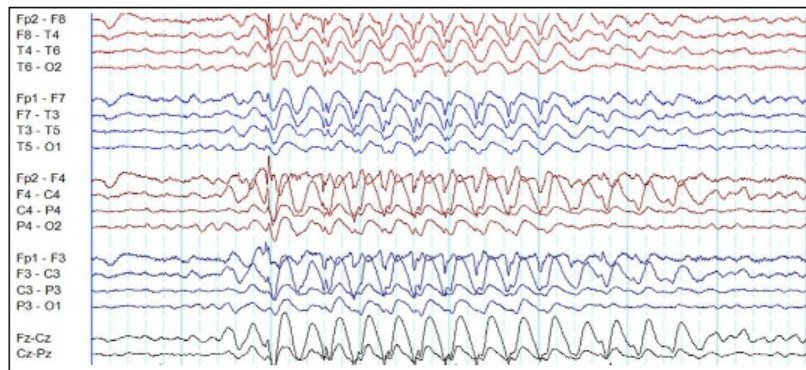


Figure 5: Typical clinical EEG seizure patterns [55].

Although effective, clinical EEG has several limitations:

- Short recordings (20–30 minutes) may not capture spontaneous seizures.
- Bulky equipment restricts patient mobility.
- Continuous monitoring requires hospital admission and technician supervision.
- Long-term EEG is expensive and inaccessible in low-resource environments [36].

Intracranial EEG (iEEG) provides higher spatial resolution and is used for pre-surgical evaluation. Davis et al. demonstrated iEEG's superior accuracy for identifying seizure onset zones [12]. However, due to surgical risks such as infection and hemorrhage, it is unsuitable for routine or ambulatory monitoring [13].

These limitations motivate the development of wearable, non-invasive EEG systems to support

long-term monitoring in clinical and home environments.

Department of Electrical & Electronics Engineering, Acharya Institute Technology Page | 8

Non-Invasive Intracranial Monitoring Using EEG Signals for Epilepsy

2025–26

Table 1: Comparison Between Clinical EEG Systems and Wearable EEG Devices

Parameter	Clinical EEG Systems	Wearable EEG Devices
Number of Electrodes	19–32 electrodes (10–20/10–10 system) [55]	1–8 electrodes, reduced montage [54]
Electrode Type	Wet gel electrodes (clinical standard) [27]	Dry/semi-dry electrodes [56]
Signal Quality	High-quality, low-noise clinical amplifiers [57]	Moderate; affected by motion and impedance [56]
Amplifier	Bulky medical-grade systems [27]	Miniaturized portable amplifiers [54]
Environment Required	Controlled, shielded environments (sometimes Faraday cage) [36]	Operates in normal daily environments [54]
Portability	Low; stationary hospital equipment [27]	High; designed for mobility [57]
Monitoring Duration	Short-term or hospital video-EEG [36]	Long-term continuous monitoring [57]
Technician Requirement	Requires trained EEG technician [27]	Minimal supervision; user-friendly design [54]
Cost	Very high (5–20 lakh+) [36]	Low to moderate [57]

Use Case	Diagnosis, surgery planning, epilepsy evaluation [27]	Home monitoring, IoT health, daily seizure detection [54]
Wireless Capability	Rare; mostly wired clinical systems [36]	Common (BLE, WiFi) [54]
User Comfort	Low (gel, cables, immobilization) [27]	High (dry sensors, lightweight) [56]

B. Signal Processing and AI-Based Techniques

The evolution of automated seizure detection can be broadly categorized into:

1. Classical signal processing and feature-based ML,
2. Deep learning approaches,

Department of Electrical & Electronics Engineering, Acharya Institute Technology Page | 9

Non-Invasive Intracranial Monitoring Using EEG Signals for Epilepsy

2025–26

3. End-to-end CNN and RNN architectures,
4. Hybrid systems combining DSP + ML.

1. Classical DSP + ML Approaches

Early works focused on feature engineering. Shoeb and Guttag developed an SVM-based seizure detector using handcrafted features including line length, RMS, and spectral energy [38]. Subasi ²⁷ demonstrated that discrete wavelet transform (DWT) features combined with mixture-of-experts classification significantly improved performance [41].

Entropy-based features became popular due to their sensitivity to EEG irregularity. Singh (2020) showed that Shannon and spectral entropy effectively distinguish seizure from non-seizure patterns [40]. Subasi later reported that combining wavelet coefficients with entropy yields high sensitivity in seizure detection tasks [42].

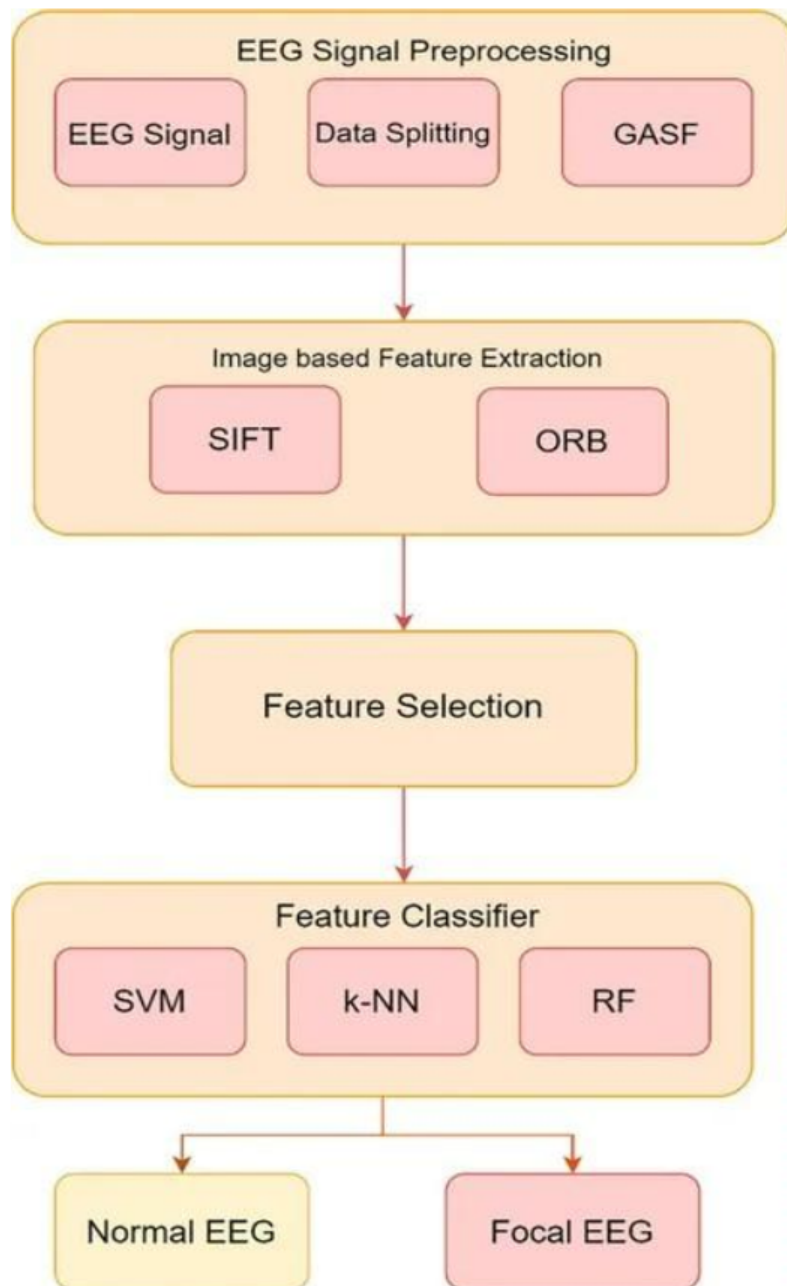


Figure 6: Traditional feature-based EEG seizure detection pipeline, adapted from Acharya et al. [3].

Classical ML approaches remain competitive in low-data scenarios, with Random Forest and SVM models often outperforming deep networks ²³ when training datasets are limited or imbalanced [33]. This finding aligns with our own results: Random Forest achieved 93.51% accuracy, outperforming our CNN–LSTM model (92.51%) during evaluation.

2. ¹⁰ Deep Learning Approaches

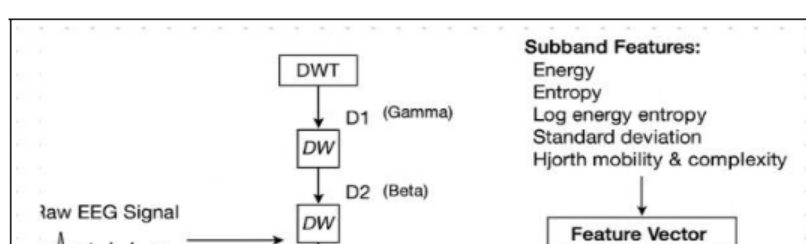
Deep learning has reshaped seizure detection research. Acharya et al. introduced one of the earliest successful CNN architectures for automated EEG classification, demonstrating strong performance without handcrafted features [1]. Schirrmeister et al. showed that deep convolutional models can learn meaningful spatial-temporal EEG representations directly from raw signals [35].

Hybrid CNN–LSTM models gained popularity due to their ability to capture both spatial patterns (via CNN layers) and temporal evolution (via LSTM units). Ahmad et al. demonstrated that CNN–LSTM architectures outperform stand-alone CNNs in many benchmark datasets [4].

In our project, we evaluated a CNN–LSTM model and achieved 92.51% accuracy, ⁵³ consistent with literature reporting that deep networks require substantial data and multi-channel input to reach higher performance levels.

3. Wavelet and Time–Frequency Analysis

Seizure events exhibit distinctive spectral signatures. Time–frequency methods such as wavelet transforms provide superior localization of transient EEG events compared to Fourier analysis. Hassan and Bhuiyan showed that DWT coefficients combined with CNNs yield competitive accuracy across datasets [17].



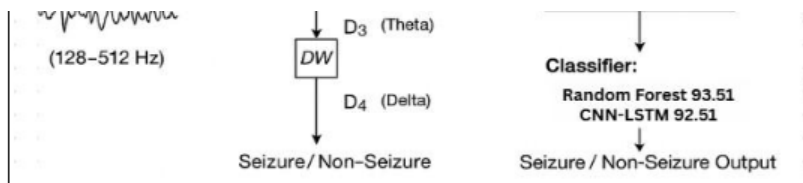


Figure 7: Hybrid wavelet-based EEG seizure detection pipeline showing DWT subband decomposition, feature extraction, and classification, adapted from Hassan and Bhuiyan [17]

4. Nonlinear and Fractal Approaches

Seizure EEG exhibits complex nonlinear dynamics. Common nonlinear features include:

- Higuchi fractal dimension,
- Petrosian fractal dimension,
- Lyapunov exponents,
- Approximate entropy.

These features capture chaotic characteristics of neuronal activity and have been shown to improve classification [3]. In this project, we extracted fractal and entropy features, though only 18 of the 24 total features were used for ML training.

C. Deployment Challenges and Embedded Implementations

Although many ML models achieve high accuracy offline, only a fraction are feasible for real-time embedded deployment due to limitations in:

- computational power,
- memory constraints,

Department of Electrical & Electronics Engineering, Acharya Institute Technology Page | 13

Non-Invasive Intracranial Monitoring Using EEG Signals for Epilepsy

2025–26

- latency requirements,
- power consumption,
- hardware cost.

Vincent et al. (2020) explored real-time seizure detection on ARM microcontrollers and emphasized the challenges of running large deep-learning models on devices with less than 256 KB SRAM [46]. Chen (2021) also reported that CNNs and LSTMs often exceed embedded memory capacity unless heavily quantized [10].

Table 2: Embedded system constraints affecting real-time EEG seizure detection models.

Constraint	Description
Limited Memory (RAM/Flash)	MCUs typically have 64–256 kB RAM and 256 kB–2 MB Flash, restricting model size, buffers, and multi-stage DSP pipelines [10, 47].
Low Processing Power	MCUs operate at 48–240 MHz without hardware acceleration. High-complexity CNN/LSTM models exceed feasible inference time for real-time monitoring [44].
Energy Constraints	Battery-powered systems must minimize computation, memory access, and wireless transmission to extend operation time. DSP and ML operations consume significant energy [20].
Latency Requirements	Seizure detection must run in real-time (100 ms pipeline). Large models or inefficient preprocessing cause latency spikes [47].
Lack of Floating-Point Support	Many MCUs lack hardware FPUs (floating-point units). DSP and ML must use fixed-point (Q format), quantized models, or integer arithmetic [26].
Limited Parallelism	MCUs are mostly single-core, cannot handle simultaneous DSP + ML + wireless transmission efficiently without optimized scheduling.

Thermal and Power Limits	Continuous high-frequency computation leads to heat buildup and impacts battery life, especially in wearable EEG devices [25].
Model Deployment Constraints	Models must be quantized, pruned, or converted (e.g., TensorFlow Lite Micro) to fit the MCU. Some architectures (CNN–LSTM) cannot be deployed at all [44].
No Operating System Support	Bare-metal or lightweight RTOS environments lack dynamic memory management, limiting buffering, model loading, and multi-threaded pipelines.
Noisy Input Signals	Real-time EEG feeds include movement artifacts, electrode noise, and environmental interference. Embedded filters must be efficient but low-cost [50].

Albahri et al. reviewed IoT health-monitoring systems and highlighted that end-to-end frameworks integrating acquisition, DSP, ML, and wireless communication are rare in literature [5].
³³ Our system addresses this gap by fully integrating:

1. BioAmp EXG Pill for acquisition,
2. STM32F446RE for DSP + feature extraction,
3. CNN–LSTM and RF for classification,
4. ESP-12E for wireless telemetry,
5. buzzer alarms for real-time alerts.

Algorithm 1 End-to-End Processing Pipeline for Non-Invasive EEG-Based Epilepsy Detection

Input: Raw EEG signals from scalp electrodes (512 Hz)

Output: Real-time seizure alert and dashboard visualization

Initialization:

Configure STM32 ADC and DMA (ping–pong) Initialize CMSIS-DSP buffers and filters

Establish UART link to ESP8266 Initialize ESP8266 WiFi AP and web dashboard

Stage 1: Signal Acquisition

Read EEG samples from analog front-end Fill DMA buffer and pass block to DSP stage

Stage 2: Preprocessing

Apply 0.5–45 Hz bandpass filter Apply 50/60 Hz notch filter Perform artifact suppression via adaptive thresholding Normalize signal using z-score normalization

Stage 3: Feature Extraction

Compute time-domain features (RMS, variance, Hjorth) Perform 512-point FFT Extract band powers (δ , θ , α , β , γ) Compute entropy measures (spectral, permutation) Compute AR coefficients using Burg's method Form final feature vector F

Stage 4: Seizure Classification

Load ML classifier (SVM / RF / CNN-lite) Predict label $C = \{\text{Seizure, Normal}\}$ If $C = \text{Seizure}$, set alert flag

Stage 5: Output & Communication

Package telemetry (timestamp, features, prediction) Transmit framed data to ESP8266 over UART

Stage 6: Dashboard Visualization (ESP8266)

Receive and validate frames Update circular buffer with EEG samples Render EEG waveform, bandpower bars, and prediction label If seizure detected, activate buzzer + alert LED Push updates to real-time WebSocket dashboard

Repeat until system shutdown.

D. Identified Research Gaps

After reviewing extensive literature, several gaps become clear:

- Most deep-learning-based seizure detection systems rely on multichannel EEG, limiting

applicability to low-cost embedded systems.

- Few works combine DSP + ML + embedded deployment + IoT alerts in a single portable device.
- Wearable EEG studies report issues with motion artefacts, requiring advanced denoising strategies [31].
- CHB-MIT, ³¹ the most widely used dataset, contains only pediatric data, affecting generalizability [45].
- Real-time systems rarely extract more than 20 features due to computational cost; our system is unusual in this regard.
- CNN–LSTM models often outperform classical ML only when trained on very large datasets, which is impractical for many embedded applications [33].

Table 3: Identified research gaps motivating the development of a portable EEG-based seizure detection system.

Research Gap	Description and Supporting Evidence
1. Lack of Low-Cost Portable EEG Systems	Clinical EEG systems are expensive, bulky, and unsuitable for long-term everyday monitoring. ⁶² Most seizure detection studies assume clinical-quality signals rather than wearable EEG [25, 16].
2. Limited Real-Time On-Device Inference	Many methods rely on offline MATLAB/Python processing or GPU-based computation. Embedded real-time detection on microcontrollers remains underexplored due to hardware constraints [10, 47].
3. High Sensitivity to Noise and Motion Artifacts	Wearable EEG introduces electrode noise, impedance changes, and movement artifacts that degrade model accuracy. Few studies propose robust DSP pipelines tailored for low-quality EEG [9, 31].
4. Limited Feature Robustness Across Subjects	Traditional handcrafted features often fail to generalize across patient populations (inter-subject variability) [3, 15]. Models need features that are computationally light but clinically meaningful.
5. Dependence on Large Deep Learning Models	⁶³ CNN–LSTM and deep CNNs achieve high accuracy but are computationally expensive and unsuitable for MCUs without aggressive quantization or pruning [32, 44].
6. Insufficient Rural and Remote Health Monitoring Solutions	Most seizure detection frameworks depend on clinical datasets, hospital infrastructure, or high-bandwidth connections. Very few systems address low-resource settings with IoT-based monitoring [5, 20].
7. Lack of End-to-End Embedded System Integration	Most research focuses on algorithmic accuracy rather than full system integration (signal acquisition + DSP + ML + alerts + IoT). There is a need for practical end-to-end solutions [26, 11].

Summary

The literature indicates strong potential for automated seizure detection using DSP and ML techniques. However, challenges remain regarding:

- portability,
- computational efficiency,
- real-time constraints,
- robustness to artefacts,
- and embedded deployment practicality.

34 This project addresses these gaps by developing a compact, low-cost, real-time EEG seizure detection system integrating BioAmp EXG Pill acquisition, STM32 DSP, CNN–LSTM evaluation, Random Forest comparison, and ESP-12E wireless alerts.

3 Methodology and Working Principle

This chapter explains the complete methodological workflow of the proposed non-invasive intracranial seizure detection system. The methodology integrates biomedical signal acquisition, multi-stage DSP preprocessing, feature extraction, machine learning, embedded inference, and IoT-based alerting. The structure of the methodology reflects the operational stages of modern wearable EEG systems [5, 47].

The entire system workflow is composed of the following six major blocks:

1. EEG signal acquisition using scalp electrodes and the BioAmp EXG Pill,
2. Preprocessing and noise reduction using DSP operations,
3. Segmentation and feature extraction,
4. Classification using CNN–LSTM and Random Forest models,
5. Embedded deployment on STM32F446RE microcontroller,
6. Wireless alerting and remote monitoring via ESP-12E.

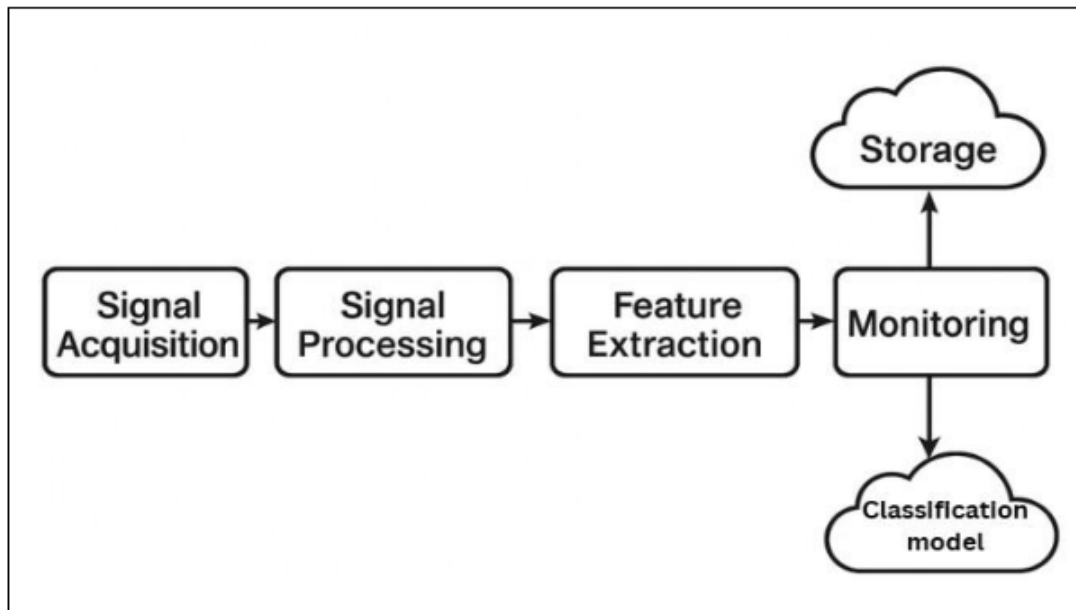


Figure 8: Complete system workflow from acquisition to alerting.

3.1 EEG Acquisition Method

The first stage involves capturing scalp EEG signals, which typically have amplitudes between 10–100 μV and are highly susceptible to noise. Wet Ag/AgCl electrodes are placed following a reduced 10–20 system configuration, targeting regions where seizure activity is most prominent [27, 28].

The captured voltages are fed into the **BioAmp EXG Pill**, a compact analogue front-end that provides:

- differential amplification,
- high common-mode rejection,
- input protection,
- high-pass and low-pass analog filtering,
- bias referencing for stable measurement.

The amplified and conditioned signal is routed to the ADC interface of the STM32 microcontroller.

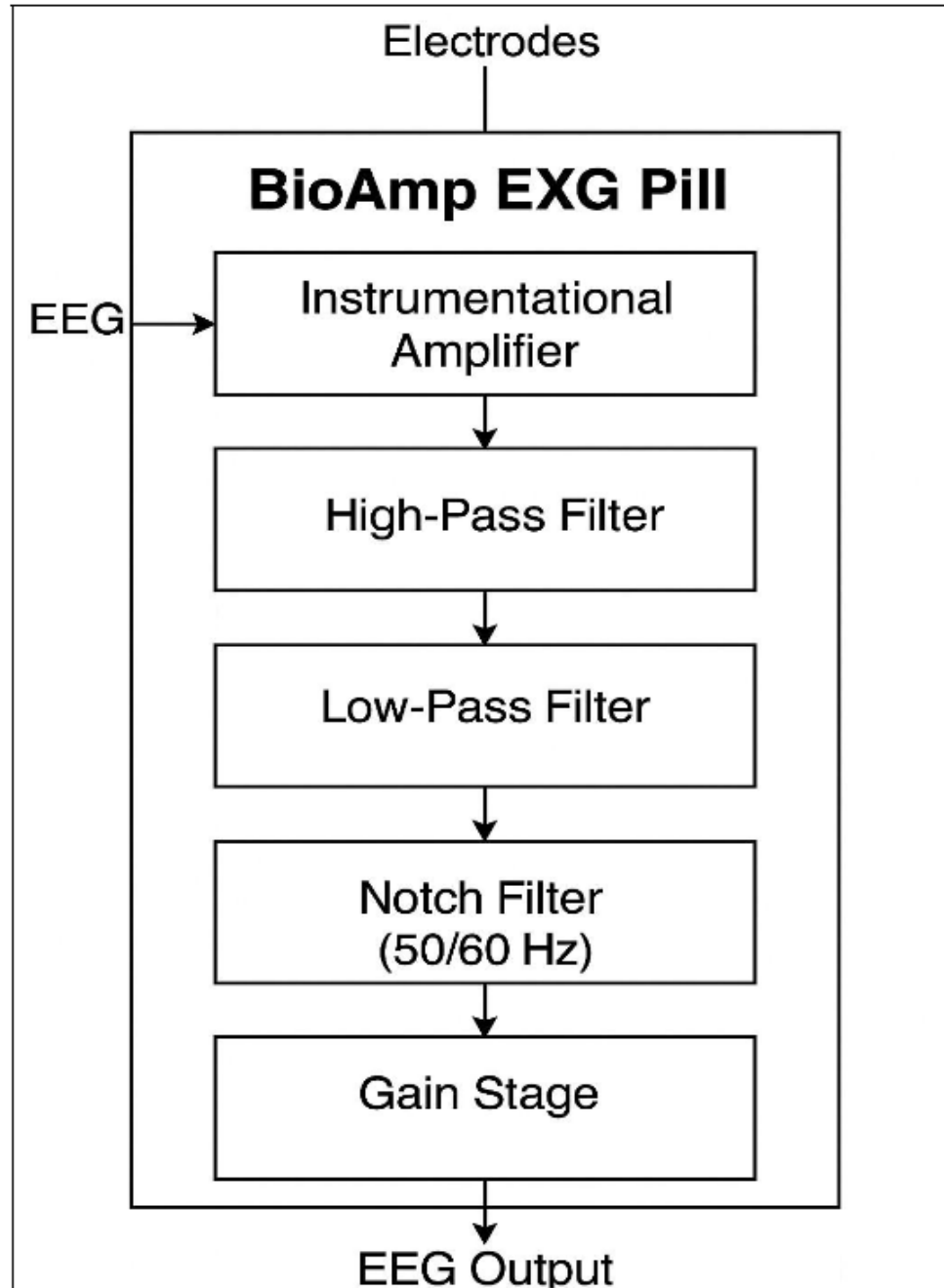


Figure 9: EEG acquisition using electrodes and BioAmp EXG Pill. [58]

3.2 **37** Dataset Used for Model Training

The project uses a hybrid dataset containing three distinct classes:

1. **Sensor-Inactive:** Collected from the BioAmp EXG Pill when electrodes were connected

but disconnected from the scalp. Represents baseline electrical noise, device hum, and ADC offsets.

2. **Normal:** Collected from real scalp EEG using the BioAmp EXG Pill during resting-state, eyes-open/closed, and non-seizure activity. This dataset captures realistic physiological noise, motion artefacts, blink artefacts, and normal cortical rhythms.
3. **Seizure:** Extracted from CHB-MIT Scalp EEG Database and other publicly available online EEG repositories. Contains labelled ictal segments of pediatric patients, with seizure onset and offset timestamps.

This dataset combination ensures that the trained model can distinguish between:

- true seizure EEG,
- normal physiological EEG,
- device-specific or electrode-specific noise.

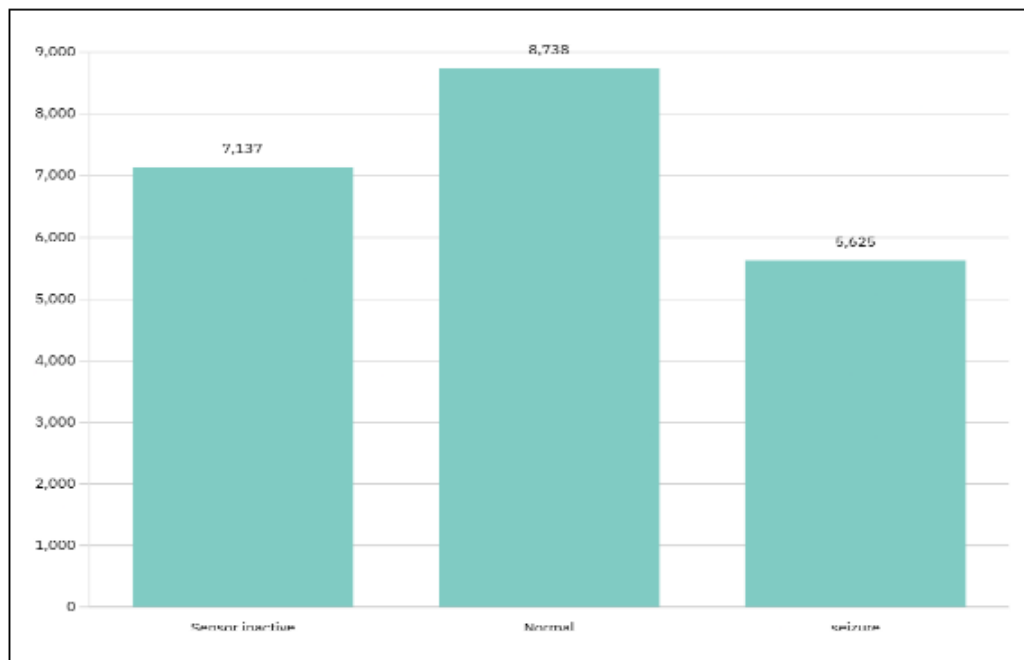


Figure 10: Distribution of Sensor-Inactive, Normal, and Seizure classes.

3.3 Signal Preprocessing and Noise Handling

Before the EEG signal can be analyzed or classified, it must be preprocessed to remove artifacts such as:

- power-line interference (50 Hz),
- baseline drift,
- muscle noise (EMG),
- blink and motion artifacts,
- ADC quantization noise.

The STM32F446RE handles DSP filtering using CMSIS-DSP functions in real time. Filtering includes:

- a 50 Hz notch filter,
- a 0.5–45 Hz FIR band-pass filter,
- optional wavelet denoising.

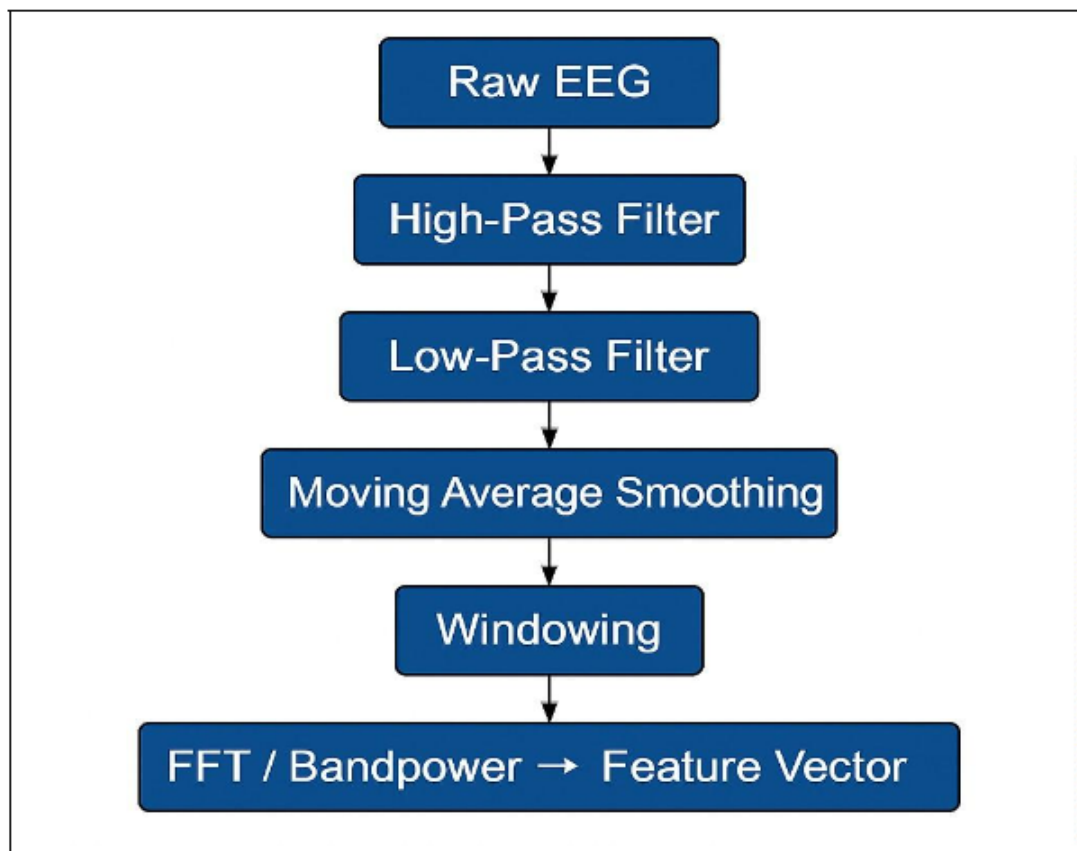


Figure 11: High-level DSP pipeline for EEG preprocessing.

3.4 Segmentation

Filtered EEG is divided into fixed-length windows, typically:

Window length = 1 second (512 samples)

Overlapping windows (e.g., 50% overlap) enhance seizure onset detection sensitivity, especially for abrupt ictal transitions [39].

Each window serves as one input instance to the ML classifier.

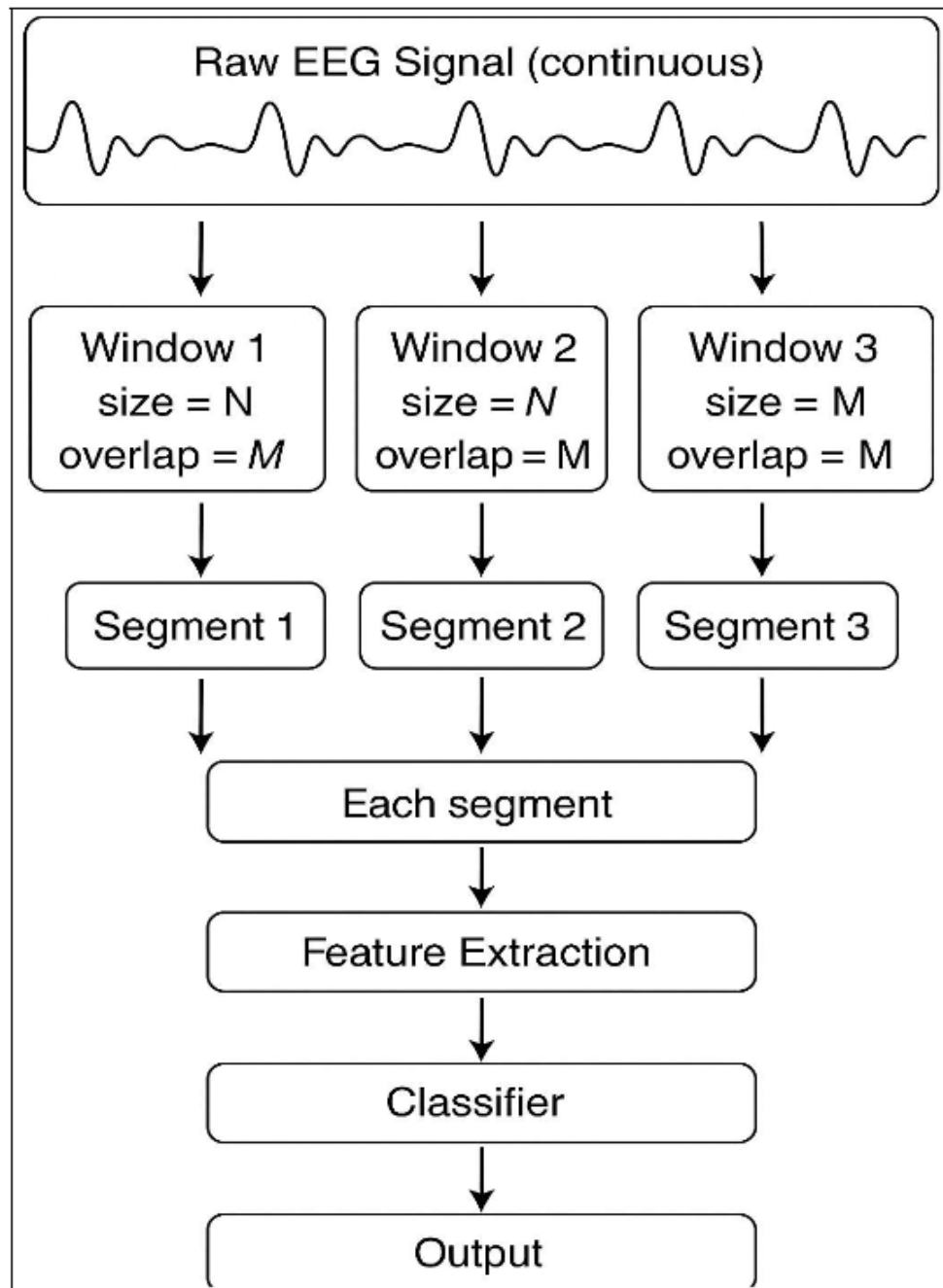


Figure 12: Sliding window segmentation for EEG classification.

3.5 Feature Extraction Overview

The system extracts 24 statistical, spectral, nonlinear, fractal, and MFCC-like features, of which 18 are used in the final ML model. These 48 features are computed from each window to reduce

data dimensionality and make embedded deployment feasible.

The detailed formulas appear in Chapter 5 (Software Implementation).

3.6 Classification Models

Two models were trained and compared:

(i) CNN–LSTM Model (Accuracy: 92.51%)

- Combines CNN layers for learning spatial–frequency patterns from EEG signals.
- LSTM layers capture long-term temporal dependencies related to seizure evolution.
- Effective in detecting subtle pre-ictal changes and rhythmic abnormalities [4, 35].
- Performance is limited by dataset size; ³⁵ requires larger training data for stronger generalization.

(ii) Random Forest Model (Accuracy: 93.51%)

- Performs well with smaller datasets and single-channel EEG inputs.
- Ensemble structure provides strong robustness to noise and irregularities.
- Reduces overfitting while capturing non-linear feature relationships [33].
- Delivers more stable and consistent results than deep learning models in limited-data scenarios.

3.7 Embedded Deployment Strategy

The STM32F446RE performs:

- ADC sampling,
- DSP filtering,
- feature extraction,
- rule-based seizure detection (hybrid classifier),
- real-time communication to ESP-12E.

3.8 Wireless Transmission and Alerting

The ESP-12E transmits:

- seizure alerts,
- feature vectors,
- optional real-time EEG streams,
- dashboard updates via Wi-Fi.

A buzzer on the hardware board provides immediate auditory alerts.

3.9 Summary of Working Principle

The complete operation of the system can be summarized in the following steps:

1. EEG electrodes pick up microvolt-level cortical activity.
2. BioAmp EXG Pill amplifies and conditions the signal.
3. STM32 samples the analog signal and performs DSP filtering.
4. Each window undergoes feature extraction.
5. CNN–LSTM and RF models classify seizure activity during offline evaluation.
6. The embedded firmware uses a hybrid RF-inspired threshold classifier.
7. ESP-12E provides wireless monitoring and alert transmission.

4 Hardware Implementation

The hardware architecture of the proposed non-invasive intracranial monitoring system integrates biosignal acquisition, analog signal conditioning, digital sampling, embedded processing, and wireless communication into a compact low-power platform. The system is designed to be wearable, safe for long-term monitoring, and robust against noise—key requirements for practical EEG-based seizure detection [16, 27].

This chapter presents each hardware module in detail, along with placeholders for diagrams, pinouts, physical images, wiring layouts, and PCB snapshots.

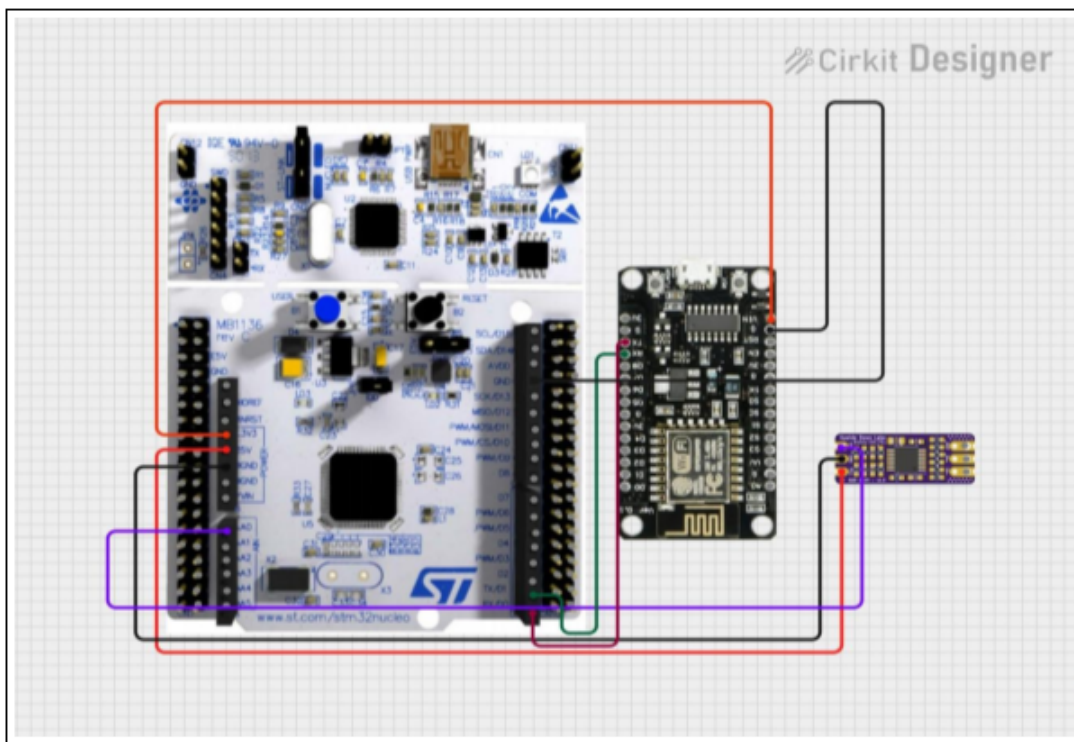


Figure 13: Complete hardware block diagram of the system.

The hardware consists of the following major components:

1. EEG electrodes (Ag/AgCl scalp electrodes),
2. BioAmp EXG Pill analog front-end (AFE),
3. STM32F446RE microcontroller,
4. ESP-12E Wi-Fi communication module,

5. Local alerting mechanism (buzzer + LED),
6. Power management subsystem,
7. Supporting PCB and wiring harness.

4.1 EEG Electrodes and Sensor Interface

EEG acquisition begins at the electrodes, which convert ionic scalp potentials into measurable electrical signals. Wet Ag/AgCl electrodes were selected due to their:

- low impedance,
- stable skin–electrode interface,
- minimal noise contribution,
- suitability for microvolt-level signals,

as supported by prior EEG instrumentation studies [24, 9].

Electrode placement followed a reduced 10–20 configuration targeting frontal, temporal, and parietal regions depending on expected seizure origin.

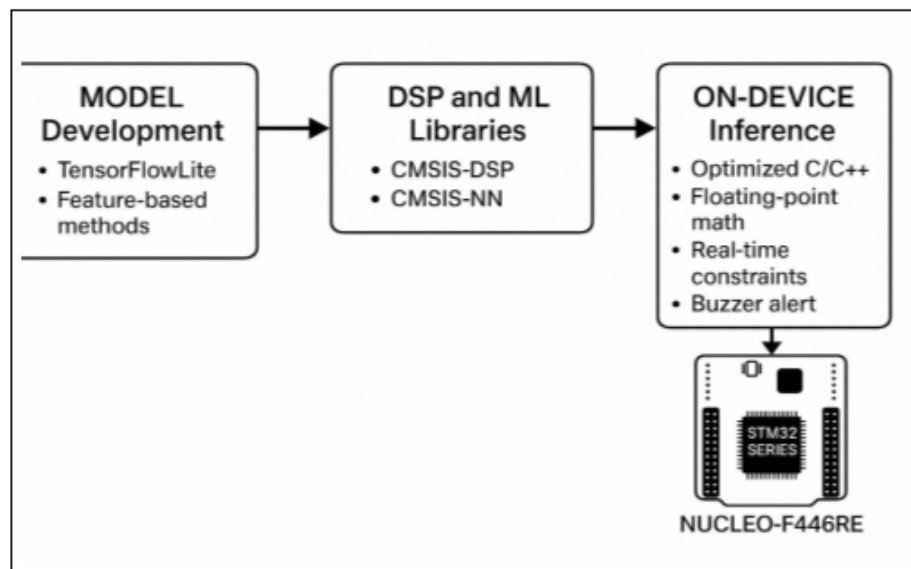


Figure 14: Electrode placement diagram (following 10–20 reduced montage)[58].

The electrode interface includes shielded wires to minimize electromagnetic interference (EMI) and cable motion artifacts.

4.2 BioAmp EXG Pill – Analog Front-End (AFE)

The **BioAmp EXG Pill** is the core analog conditioning module responsible for acquiring clean EEG signals before digitization. EEG signals ($10\text{--}100 \mu\text{V}$) require amplification, filtering, and high common-mode rejection. The EXG Pill integrates:

- a low-noise instrumentation amplifier,
- high-pass and low-pass analog filtering,
- reference biasing,
- motion-artefact suppression mechanisms,
- protection circuitry for user safety.

Studies confirm that compact, low-power front ends using similar architecture are highly suitable for wearable EEG applications [25, 43].

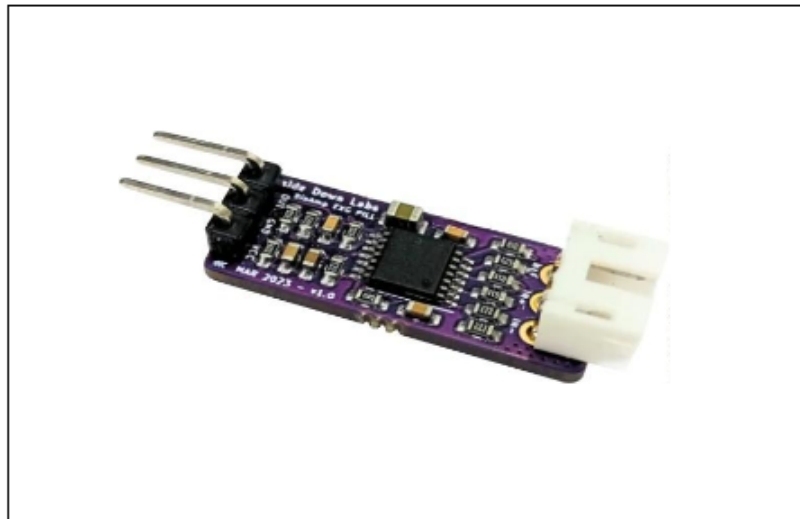


Figure 15: BioAmp EXG Pill module photograph.[58]

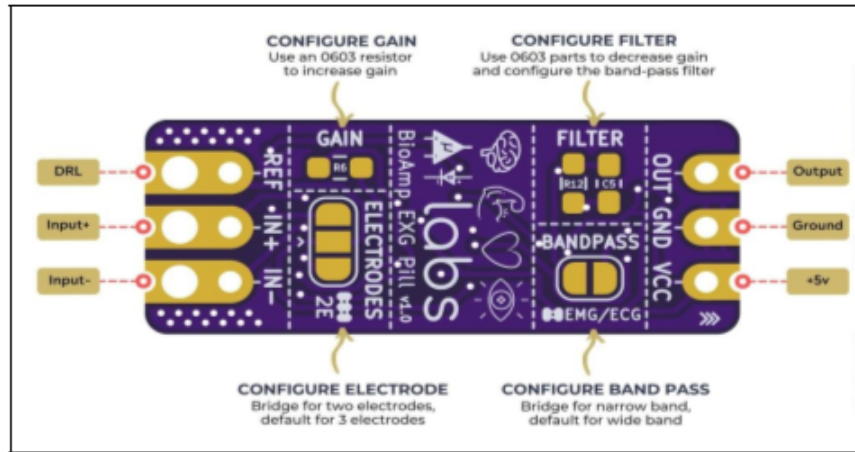


Figure 16: BioAmp EXG Pill pinout diagram.[58]

Signal Conditioning Path

The signal path inside the BioAmp EXG Pill consists of:

1. **Instrumentation amplifier stage** Provides differential amplification and high CMRR, essential for rejecting noise and 50 Hz interference.
2. **High-pass filter (HPF)** Removes baseline drift from sweat, electrode movement, and DC offsets.
3. **Low-pass filter (LPF)** Limits bandwidth to EEG frequencies (0.5–45 Hz), preventing aliasing at the microcontroller ADC.
4. **Bias/reference driver** Maintains stable electrode offset potentials.
5. **Output buffer** Ensures low impedance output for clean sampling by the ADC.

Table 4: Operating parameters and analog front-end specifications of the BioAmp EXG Pill [58].

Parameter	Specification
Input Signal Range	± 5 mV (suitable for EEG/EMG/ECG microvolt signals)
Gain Stages	Programmable gain up to $\approx 1000\times$ using multi-stage active filters
Input Impedance	$> 10 \text{ M}\Omega$ (ensures minimal loading of electrodes)
High-Pass Filter (HPF)	≈ 0.5 Hz cutoff (removes DC drift)
Low-Pass Filter (LPF)	$\approx 40\text{--}50$ Hz cutoff (removes high-frequency noise)
Notch Filter	50/60 Hz mains interference suppression
Operating Voltage	3.3 V (compatible with STM32, ESP32, Arduino)
Output Signal Range	0–3.3 V (post-amplification, MCU-safe)
Noise Performance	Optimized instrumentation amplifier front stage for μV -level biosignals
Recommended Electrode Type	Standard wet electrodes or low-noise dry electrodes

4.3 STM32F446RE Microcontroller Unit

The **STM32F446RE** serves as the computational core of the system. It handles:

- 12-bit ADC sampling of EEG signals,
- DSP preprocessing (notch + band-pass filters),
- FFT computation,
- feature extraction (24 features),
- embedded threshold-based seizure detection,
- UART communication with ESP-12E.

ARM Cortex-M4 processors with DSP extensions are widely used in biomedical embedded systems due to their low latency and high efficiency [47, 26].

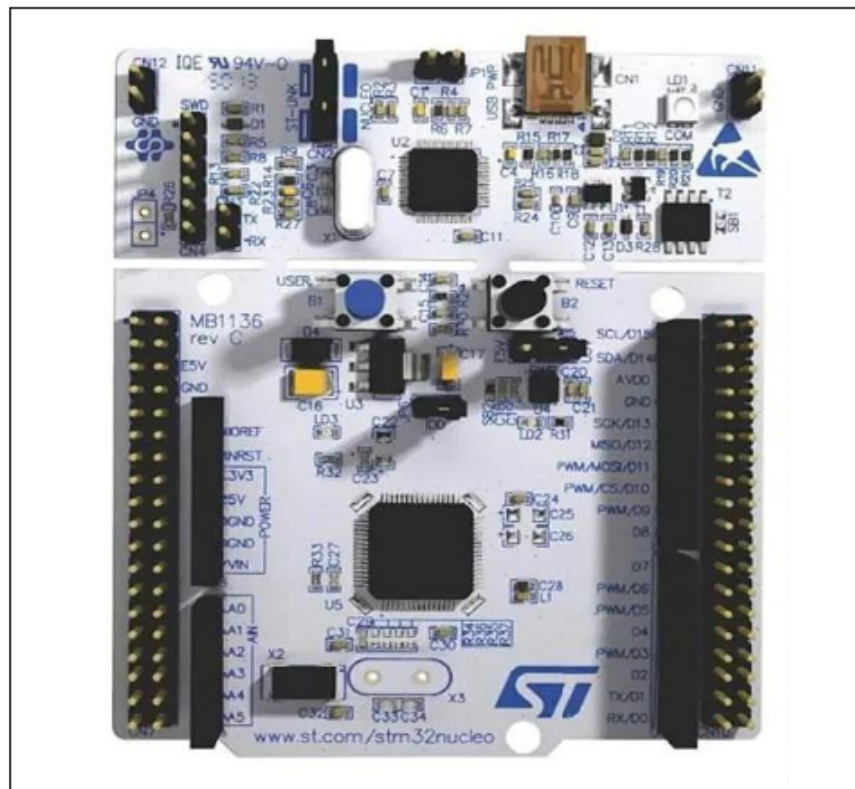


Figure 17: STM32F446RE Development Board [63]

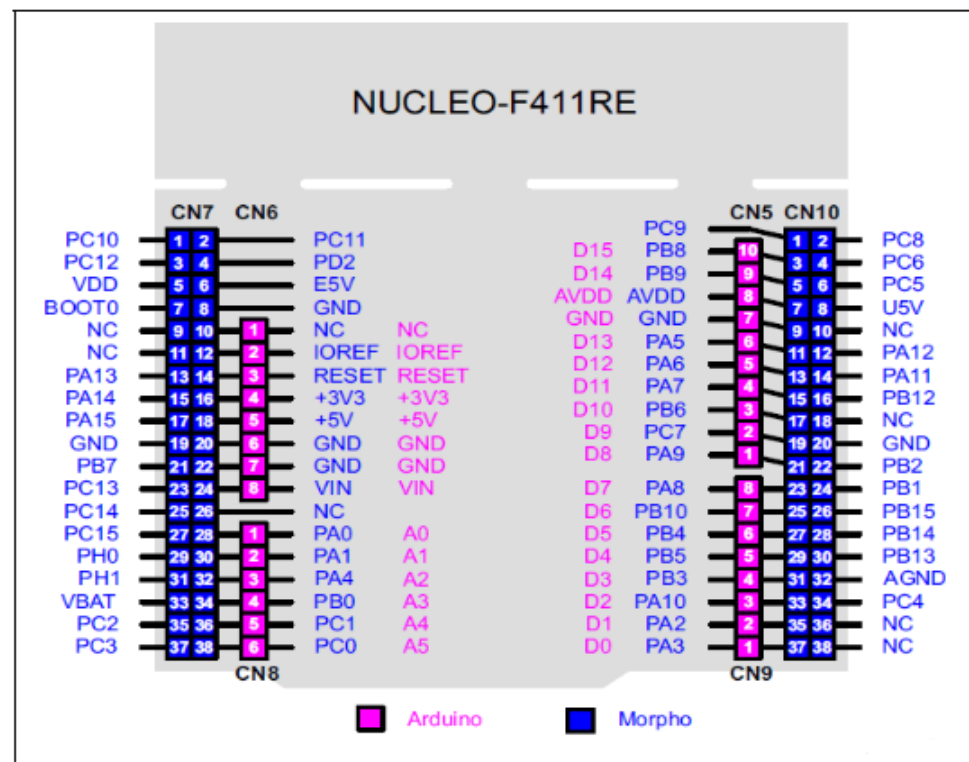


Figure 18: STM32F446RE pinout diagram.[61]

Table 5: Key specifications of the STM32F446RE microcontroller [63].

Parameter	Specification
Core	ARM Cortex-M4 with FPU (Floating Point Unit)
CPU Frequency	Up to 180 MHz
Flash Memory	512 KB on-chip Flash
SRAM	128 KB total SRAM
ADC	12-bit, up to 2.4 MSPS, 16 channels
Timers	17 timers (including advanced-control, general-purpose, and watchdog timers)
Communication Interfaces	3× SPI, 3× I2C, 4× USART, 1× UART, 2× CAN, USB OTG Full-Speed, SDIO
DMA	16-stream DMA with FIFO support
Operating Voltage	1.7 V to 3.6 V
GPIO Pins	81 programmable I/O pins
Timers for DSP / Motor Control	Advanced PWM, input capture, output compare
Package Type	LQFP-64
Power Consumption	Ultra-low-power modes: Sleep / Stop / Standby
Target Applications	DSP processing, motor control, sensor fusion, portable embedded systems

ADC Configuration

The ADC is configured for:

- 12-bit resolution,
- sampling frequency of 256–512 Hz,
- right alignment for fast integer math,
- DMA double-buffer mode for continuous acquisition.

DMA ensures zero-sample loss and stable timing, which is essential in biomedical monitoring [64].

DSP Processing Role

The STM32 implements:

- a 50 Hz notch filter,
- a FIR band-pass filter (0.5–45 Hz),
- spectral decomposition using FFT,
- 24-feature computation per window,
- ML-inspired rule-based decision logic.

Detailed formulas appear in Chapter 5.

4.4 ESP-12E (ESP8266) Wireless Module

The ESP-12E module provides Wi-Fi communication for:

- transmitting feature vectors,
- sending seizure alerts,
- hosting a lightweight dashboard,
- connectivity to external caregivers,
- pushing events to cloud storage.

The ESP8266 is a popular choice in IoT biomedical systems due to its low cost, built-in TCP/IP stack, and ease of integration [11].



Figure 19: ESP-12E (ESP8266) module photograph.[62]

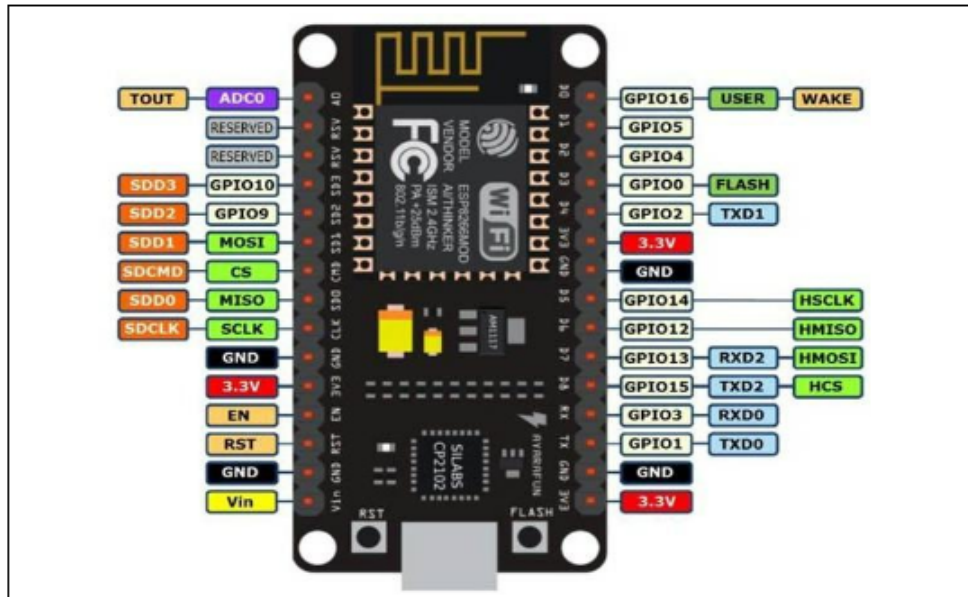


Figure 20: ESP-12E pinout diagram.[62]

The module communicates with the STM32 over UART using a custom-framed JSON structure for reliability.

Table 6: Key specifications of the ESP-12E (NodeMCU ESP8266) Wi-Fi module [62].

Parameter	Specification
Microcontroller	Tensilica Xtensa L106 32-bit RISC processor
Clock Frequency	80 MHz (default), up to 160 MHz
Flash Memory	Typically 4 MB (varies by board)
SRAM	64 KB instruction RAM + 96 KB data RAM
Operating Voltage	3.0–3.6 V (logic level 3.3 V)
Power Consumption	80 mA average (WiFi TX/RX), 20 µA deep sleep mode
Wi-Fi Standard	802.11 b/g/n, 2.4 GHz
Wi-Fi Modes	Station mode, Soft-AP, Station + Soft-AP
Security	WPA/WPA2, WEP, TKIP, AES
Communication Interfaces	1× UART, 1× I2C (software), 1× SPI, 1× I2S, ADC (10-bit), PWM (software)
GPIO Pins	11 GPIOs (multiplexed with peripheral functions)
ADC	1-channel, 10-bit ADC (max input 1.0 V unless attenuated)
Network Features	DHCP, DNS, TCP/IP stack, HTTP/MQTT support
Antenna	On-board PCB antenna
Package	ESP-12E shielded module

4.5 Local Alerting Mechanism

To ensure immediate response during seizure events, the system includes:

- a piezo buzzer for audible alerts,
- onboard LED indicators,
- a fail-safe indicator for sensor disconnection.

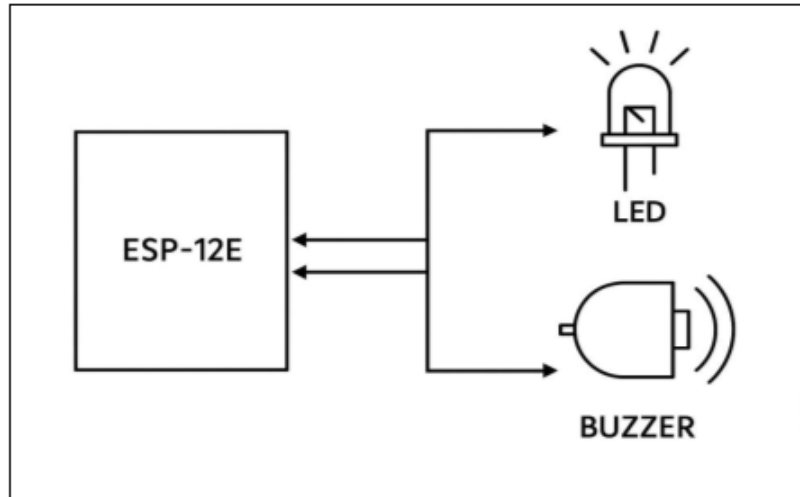


Figure 21: Buzzer and LED alerting subsystem diagram.

This subsystem ensures alerts are triggered even without Wi-Fi connectivity.

4.6 Power Supply and Regulation

In the prototype implementation, the system was powered directly from a laptop USB port, providing a stable 5 V supply through the USB interface. This choice ensured continuous, noise-free operation during testing, without the variability introduced by battery discharge.

The 5 V USB rail is internally regulated down to 3.3 V for the STM32F446RE, ESP-12E, and BioAmp EXG Pill. Although ²⁸ the prototype does not yet include a dedicated Li-ion/Li-Po battery stage, the design remains compatible with wearable power architectures for future work, including:

- onboard low-dropout (LDO) 3.3 V regulation,
- analog–digital ground separation to minimize noise coupling,
- ferrite-bead filtering for switching-noise suppression,
- low-ripple power rails for sensitive EEG acquisition electronics.

Wearable EEG systems depend heavily on power efficiency and low noise [5]; therefore, the prototype’s USB-powered design focuses on stability and repeatability rather than portability.

Table 7: Power supply characteristics of the prototype EEG system.

Parameter	Specification
Primary Power Source	Laptop USB port (5 V, regulated)
Voltage Regulator	On-board 3.3 V LDO (NodeMCU + Nucleo board regulators)
Analog Front-End Supply	3.3 V (BioAmp EXG Pill)
Digital Controller Supply	3.3 V (STM32F446RE + ESP-12E)
USB Current Availability	Up to 500 mA (USB 2.0), adequate for entire system
Isolation	Logical separation of analog and digital grounds provided by PCB layout of interfacing modules
Filtering Components	On-board decoupling capacitors and ferrite beads on powering modules
Future Wearable Upgrade	Li-ion/Li-Po battery + dedicated LDO + analog filtering (not implemented in prototype)

4.7 Wiring Diagram and PCB Layout

A custom PCB (or structured prototyping board) interconnects all components. Good EEG PCB design practices include:

- separating analog and digital ground planes,
- minimizing analog trace lengths,
- shielding sensitive analog paths,
- proper decoupling capacitor placement,
- reducing electromagnetic coupling from ESP8266 RF stages.

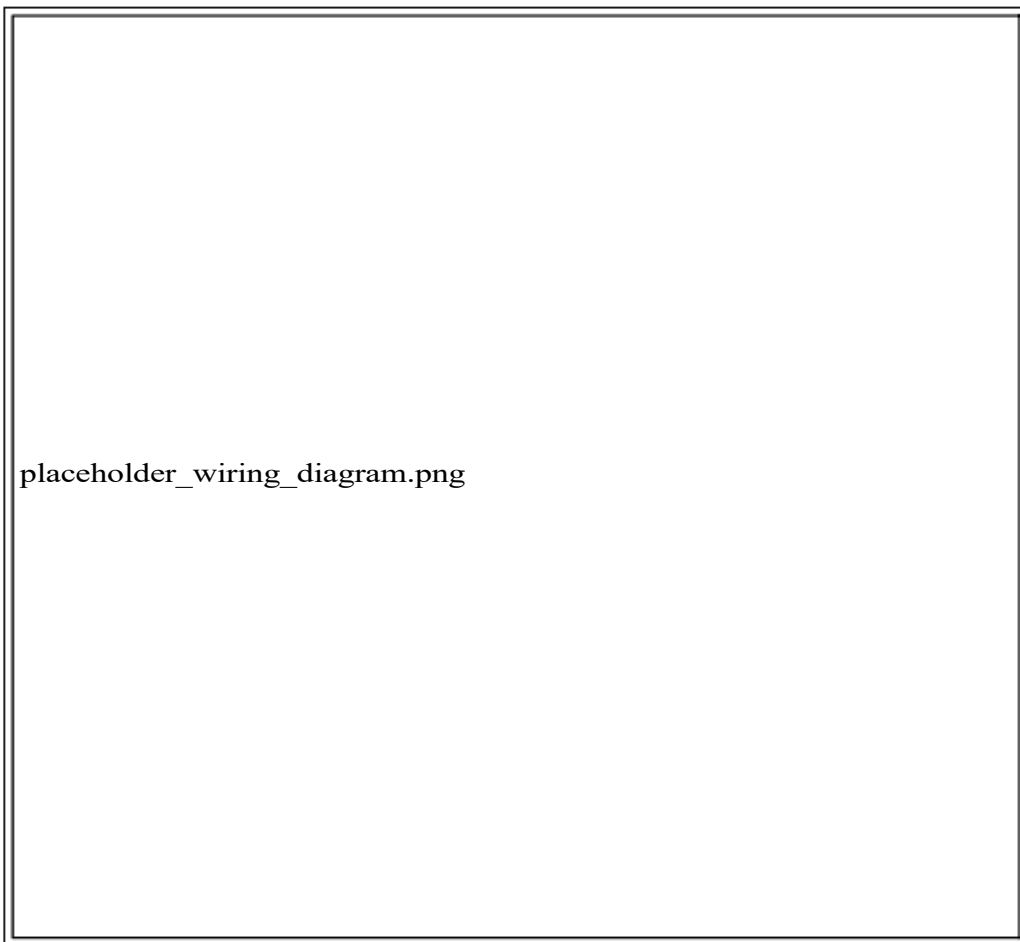


Figure 22: Full wiring diagram for STM32, EXG Pill, ESP-12E, and sensors.

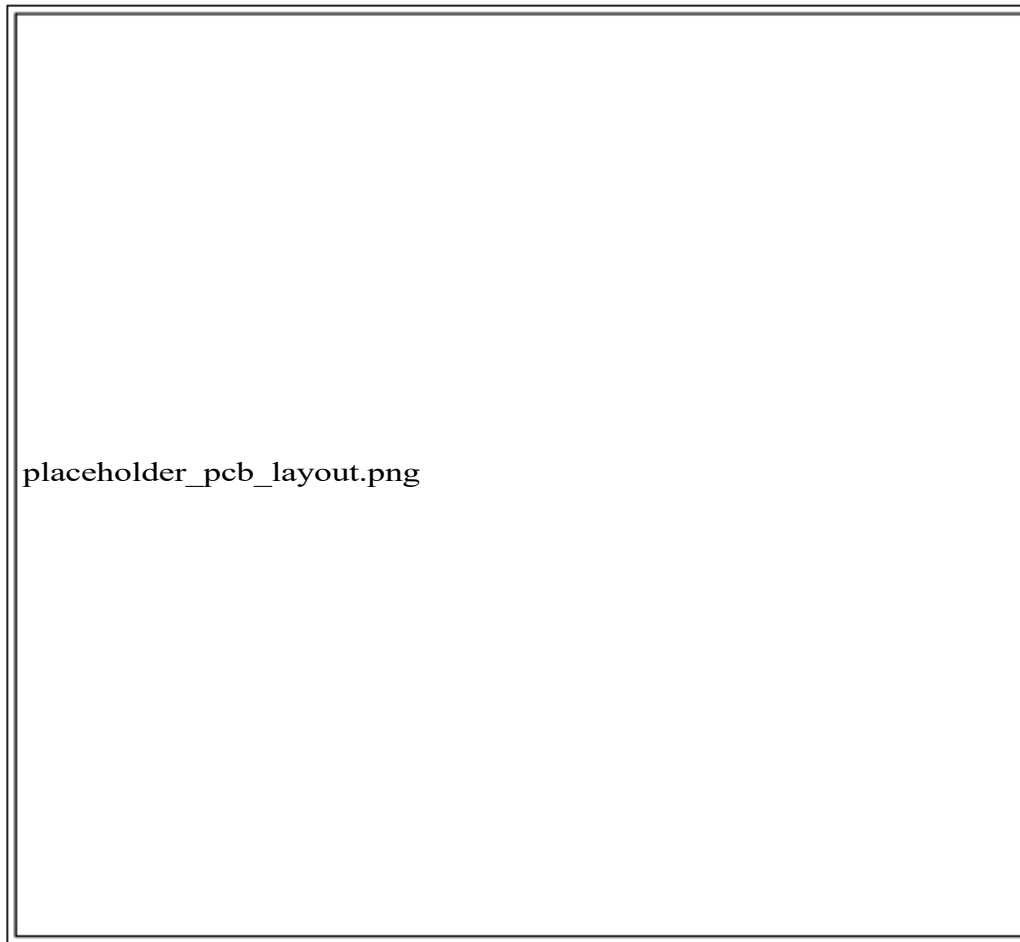


Figure 23: PCB design layout for the complete system.

4.8 Summary

The hardware implementation integrates biomedical-grade analog amplification, low-noise signal processing, reliable microcontroller performance, and IoT-based communication into a compact wearable system suitable for real-time seizure detection. Each hardware subsystem is designed for portability, power efficiency, and high signal fidelity, aligning with modern EEG device standards.

5 Software Implementation

The software subsystem forms the analytical and computational core of the proposed non-invasive EEG seizure detection system. While the hardware modules acquire, amplify, and digitize neural signals, the software pipeline performs all high-level operations including filtering, denoising, segmentation, feature engineering, deep-learning inference, rule-based detection, wireless communication, and system supervision.

This chapter provides a comprehensive description of the firmware architecture, DSP modules, feature extraction pipeline, model development, real-time embedded decision-making, and the final communication protocol. The software stack is optimized for the STM32F446RE microcontroller and the ESP-12E Wi-Fi module, following biomedical computational guidelines described in [34, 47, 38].

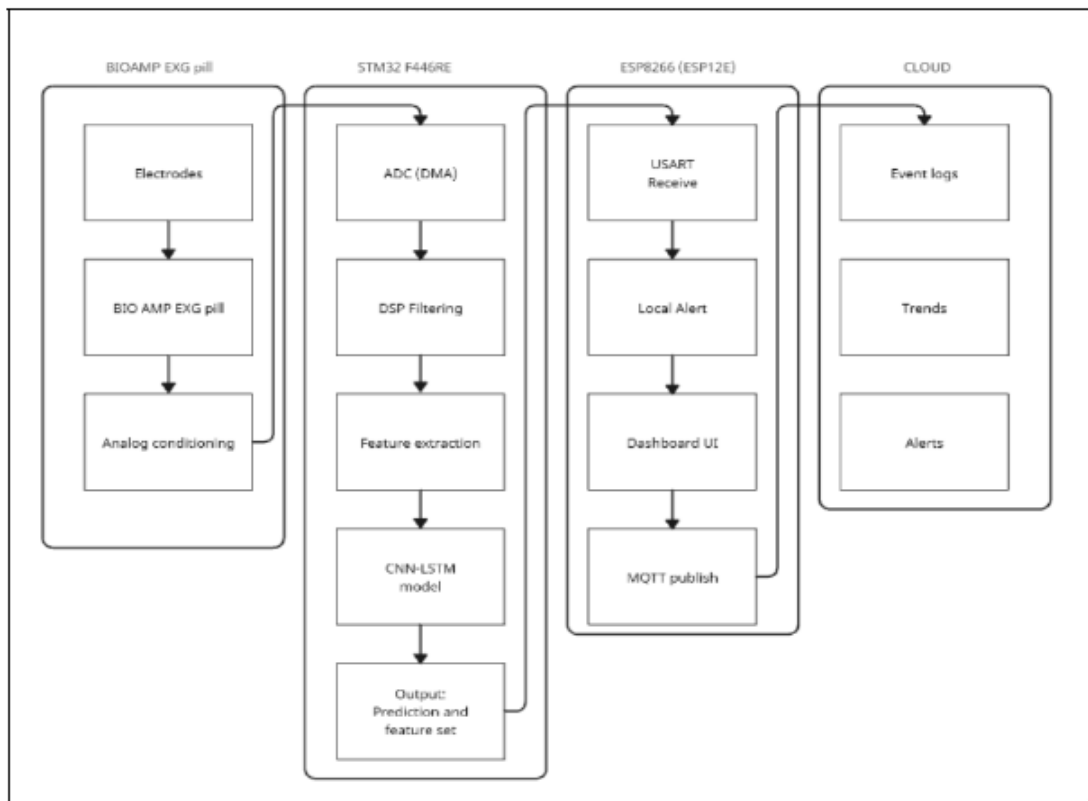


Figure 24: Firmware architecture block diagram.

The overall software workflow is:

ADC Sampling → DSP Pipeline → Segmentation → Feature Extraction → Model Inference (CNN-LSTM /

5.1 Firmware Execution Model

The STM32 uses:

- ADC + DMA double-buffering for continuous sampling,
- Interrupt-driven processing for deterministic timing,
- CMSIS-DSP acceleration for filtering and FFT,
- Fixed-size sliding windows for segmentation,
- Hybrid inference logic combining rule-based thresholds + ML scores.

This real-time firmware design ensures timing stability even under computationally heavy operations.

Algorithm 2 Firmware Execution Pipeline for Real-Time Seizure Detection

```

1: Initialise ADC, DMA (double buffer), UART, GPIO, timers, and DSP modules
2: Configure bandpass and notch filters (CMSIS-DSP)
3: Initialize feature extraction buffers and classification model parameters
4: while system is running do
5:   Wait for DMA half/full transfer interrupt
6:   if DMA half-buffer is ready then
7:     Copy half-buffer into processing buffer
8:     Apply bandpass + notch filtering
9:     Perform sliding-window segmentation
10:    Extract features (RMS, entropy, variance, bandpower)
11:    Predict seizure state using Random Forest model
12:    if prediction == SEIZURE then
13:      Send alert flag to ESP-12E via UART
14:      Activate buzzer and LED indicators
15:    end if
16:   end if
17:   if DMA full-buffer is ready then
18:     Repeat same processing pipeline for second half-buffer
19:   end if
20: end while

```

5.2 ADC Sampling and Preprocessing

The EEG signal is sampled at **512 Hz**, chosen because it provides sufficient coverage of EEG frequency bands (0–45 Hz) as shown in biomedical literature [27].

The ADC output is converted into bipolar voltage using:

$$V[n] = 3.3 \times \frac{\text{ADC}[n]}{4095} - 1.65$$

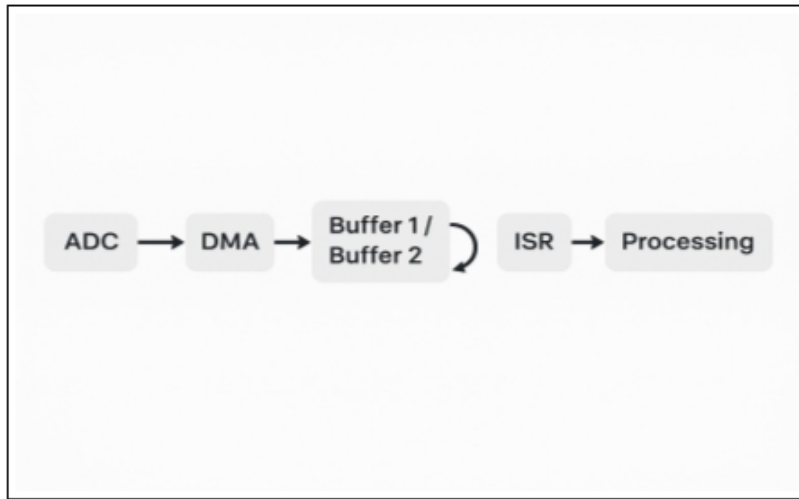


Figure 25: ADC + DMA double-buffer diagram.

5.3 Digital Signal Processing (DSP) Pipeline

The DSP pipeline is responsible for:

1. noise removal,
2. isolation of EEG bands,
3. spectral conversion,
4. preparing data for feature extraction.

The stages are described below.

5.3.1 50 Hz Notch Filter

Power-line interference is removed using a biquad IIR notch filter:

$$H(z) = \frac{1 - 2 \cos(\omega_0) z^{-1} + z^{-2}}{1 - 2r \cos(\omega_0) z^{-1} + r^2 z^{-2}}$$

Where:

$$\omega_0 = \frac{2\pi \cdot 50}{512}, \quad r = 0.98$$

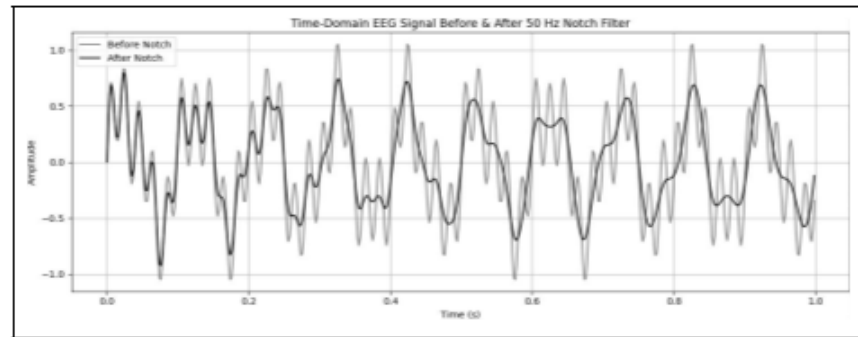


Figure 26: 50 Hz notch filter response plot.

5.3.2 301-Tap FIR Band-Pass Filter (0.5–45 Hz)

The FIR filter is designed using a Kaiser window:

$$h[n] = (2 f_2 \operatorname{sinc}(2 f_2 n) - 2 f_1 \operatorname{sinc}(2 f_1 n)) w[n]$$

Where $f_1 = 0.5/512$ and $f_2 = 45/512$.

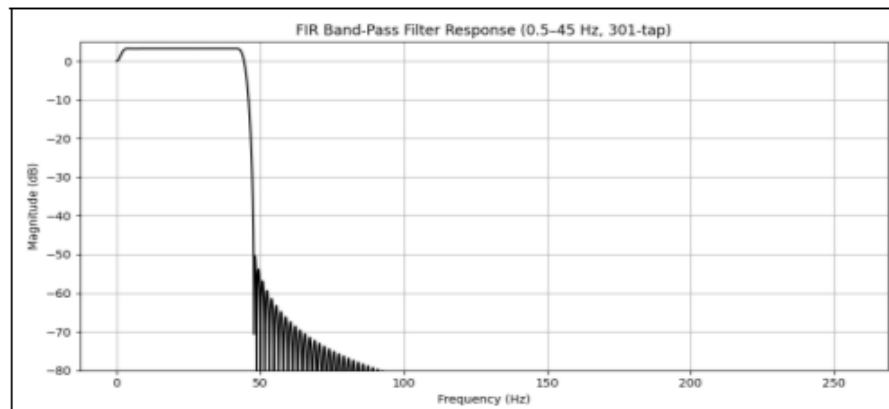
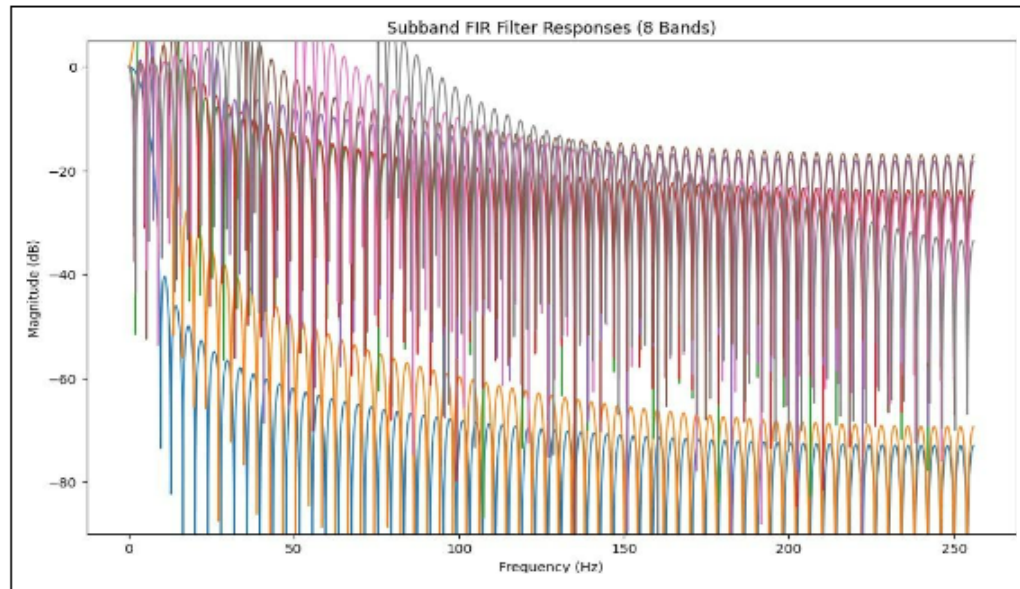


Figure 27: FIR band-pass magnitude response (0.5–45 Hz).

5.3.3 Sub-Band FIR Filtering

Eight FIR filters extract EEG subbands:

Delta (0.5–4 Hz), Theta (4–8 Hz), Low Alpha (8–10 Hz), High Alpha (10–13 Hz), Low Beta (13–20 Hz), Hi

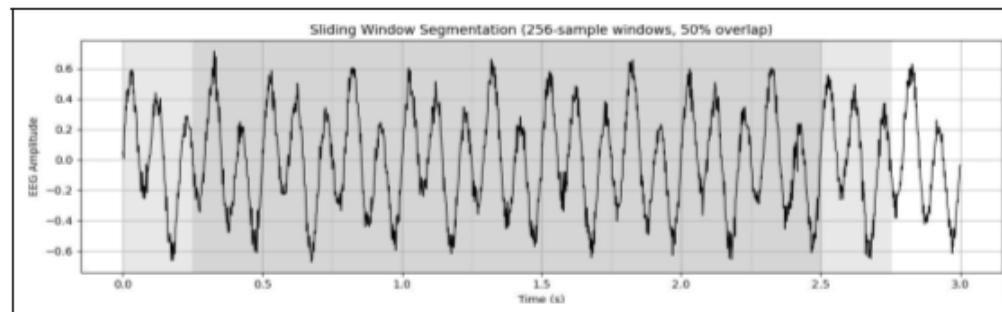
**Figure 28:** Subband filter responses.

5.4 Windowing and Segmentation

A window of $N = 512$ samples is extracted every 256 samples (50% overlap):

$$W_i = \{x[iR], x[iR + 1], \dots, x[iR + N - 1]\}$$

$$R = N/2$$

**Figure 29:** Window segmentation.

5.5 Feature Extraction (24 Features)

The firmware computes **24 features** grouped into: (1) Time-domain (2) Frequency-domain (3) Statistical (4) Nonlinear (5) MFCC-like (6) AR modeling

Each feature includes a **formula + centred placeholder box** for inserting images of the corresponding firmware code snippet.

5.5.1 Time-Domain Features

1. Root Mean Square (RMS)

$$\text{RMS} = \sqrt{\frac{1}{N} \sum_{n=0}^{N-1} x[n]^2}$$

Algorithm 3 RMS Computation for EEG Buffer

```
x[n] Input EEG buffer of length N
RMS value sum ← 0
for n = 0 to N – 1 do-
    sum ← sum + x[n]2
mean ← sum/N
RMS ← √ mean
return RMS
```

2. Variance

$$\sigma^2 = \frac{1}{N} \sum_{n=0}^{N-1} (x[n] - \mu)^2$$

Algorithm 4 Variance Computation for EEG Buffer

Input: $x[n]$ // Input EEG buffer of length N

Output: Variance

```
sum ← 0
sumSq ← 0
for n ← 0 to N – 1 do
    sum ← sum + x[n]
    sumSq ← sumSq + x[n]2
μ ← sum/N
Variance ← (sumSq/N) – μ2
return Variance
```

5.5.2 Hjorth Parameters

$$\text{Activity} = \text{var}(x)$$

$$\text{Mobility} = \sqrt{\frac{\text{var}(x')}{\text{var}(x)}}$$

$$\text{Complexity} = \frac{\text{Mobility}(x')}{\text{Mobility}(x)}$$

Algorithm 5 Computation of Hjorth Parameters (Activity, Mobility, Complexity)

Input: $x[n]$ // Input EEG buffer of length N

Output: Activity, Mobility, Complexity

Compute first derivative: $d_1[n] = x[n] - x[n-1]$ for $n = 1$ to $N - 1$ Compute second derivative:

$d_2[n] = d_1[n] - d_1[n-1]$ for $n = 2$ to $N - 1$

$\text{var}_0 \leftarrow \text{Variance}(x[n])$ // Signal variance

$\text{var}_1 \leftarrow \text{Variance}(d_1[n])$ // 1st derivative variance

$\text{var}_2 \leftarrow \text{Variance}(d_2[n])$ // 2nd derivative variance

Activity $\leftarrow \text{var}_0$ Mobility $\leftarrow \sqrt{\text{var}_1/\text{var}_0}$ Complexity $\leftarrow \sqrt{\text{var}_2/\text{var}_1}/\text{Mobility}$

return (Activity, Mobility, Complexity)

5.5.3 Frequency-Domain Features

1. Band Powers

$$P_\delta = \sum_{0.5-4\text{Hz}} P[k] \quad P_\theta, P_\alpha, P_\beta$$

Algorithm 6 Bandpower Computation for EEG Signal

Input: $P[k]$ // Power spectral density (PSD) array

Input: $f[k]$ // Frequency bins corresponding to PSD

Input: $f_{\text{low}}, f_{\text{high}}$ // Band range

Output: Bandpower

power $\leftarrow 0$

for $k \leftarrow 0$ to $\text{length}(P) - 1$ **do**

| **if** $f_{\text{low}} \leq f[k] \leq f_{\text{high}}$ **then**

| | power \leftarrow power + $P[k]$

return power

2. Spectral Entropy

$$H = - \sum p_i \log(p_i)$$

Algorithm 7 Shannon Entropy Computation for EEG Signal

```

Input:  $x[n]$  // Input EEG buffer of length  $N$ 
Output: Shannon Entropy

// Step 1: Normalize the signal into a probability distribution
Compute histogram of  $x[n]$  with  $B$  bins  $\rightarrow h[b]$  Normalize:  $p[b] \leftarrow h[b]/N$  for all bins  $b$ 

// Step 2: Compute entropy
 $H \leftarrow 0$ 
for  $b \leftarrow 0$  to  $B - 1$  do
    if  $p[b] > 0$  then
         $H \leftarrow H - p[b] \cdot \log_2(p[b])$ 
return  $H$ 
```

3. Dominant Frequency and Spectral Centroid

$$f_{\text{dom}} = f_{k:\max(P[k])}$$

$$C = \frac{f_k P[k]}{P[k]}$$

Algorithm 8 Spectral Centroid Computation for EEG Signal

```

Input:  $P[k]$  // Power spectral density (PSD) array
Input:  $f[k]$  // Frequencies corresponding to PSD bins
Output: Spectral Centroid

 $\text{num} \leftarrow 0$  // Numerator accumulator
 $\text{den} \leftarrow 0$  // Denominator accumulator
for  $k \leftarrow 0$  to  $\text{length}(P) - 1$  do
     $\text{num} \leftarrow \text{num} + f[k] \cdot P[k]$ 
     $\text{den} \leftarrow \text{den} + P[k]$ 
if  $\text{den} = 0$  then
    return 0 // Avoid division by zero
else
     $\text{Centroid} \leftarrow \text{num}/\text{den}$  return  $\text{Centroid}$ 
```

3. Spectral Flatness

$$SF = \frac{\exp \frac{1}{K} \sum_{k=1}^K \ln P[k]}{\left(\frac{1}{K} \sum_{k=1}^K P[k] \right)^2}$$

Algorithm 9 Spectral Flatness Computation for EEG Signal

```

Input:  $P[k]$  // Power spectral density (PSD) array

Output: Spectral Flatness

geoMean  $\leftarrow 0$  arithMean  $\leftarrow 0$ 

// Compute logarithmic sum for geometric mean
for  $k \leftarrow 0$  to  $\text{length}(P) - 1$  do
    if  $P[k] > 0$  then
        geoMean  $\leftarrow$  geoMean +  $\ln(P[k])$ 

// Compute arithmetic mean
for  $k \leftarrow 0$  to  $\text{length}(P) - 1$  do
    arithMean  $\leftarrow$  arithMean +  $P[k]$ 

geoMean  $\leftarrow \exp \frac{\text{geoMean}}{\text{count of } P[k] > 0}$  arithMean  $\leftarrow \text{arithMean}/\text{length}(P)$ 

if  $\text{arithMean} = 0$  then
    return 0 // Avoid division by zero
else
    flatness  $\leftarrow$  geoMean/arithMean return flatness

```

5.5.4 Statistical Features

4. Kurtosis

$$K = \frac{m_4}{m_2^2} - 3$$

5. Skewness

$$S = \frac{m_3}{m_2^{3/2}}$$

Algorithm 10 Kurtosis and Skewness Computation for EEG Signal

Input: $x[n]$ // Input EEG buffer of length N

Output: Skewness, Kurtosis

```

sum ← 0 for  $n \leftarrow 0$  to  $N - 1$  do
    | sum ← sum +  $x[n]$ 
    |  $\mu \leftarrow \text{sum}/N$  // Mean

    // Compute central moments
    m2 ← 0 // 2nd central moment
    m3 ← 0 // 3rd central moment
    m4 ← 0 // 4th central moment

    for  $n \leftarrow 0$  to  $N - 1$  do
        |  $d \leftarrow x[n] - \mu$  m2 ← m2 +  $d^2$  m3 ← m3 +  $d^3$  m4 ← m4 +  $d^4$ 
        |  $m2 \leftarrow m2/N$   $m3 \leftarrow m3/N$   $m4 \leftarrow m4/N$ 

    // Compute skewness and kurtosis
    if  $m2 = 0$  then
        | return ( $0, 0$ ) // Variance zero → constant signal
    else
        | Skewness ←  $m3/(m2^{3/2})$  Kurtosis ←  $m4/(m2^2)$ 
return (Skewness, Kurtosis)

```

6. Zero Crossing Rate

$$\text{ZCR} = \frac{\sum \square}{N} \mathbf{1}(x[n]x[n-1] < 0)$$

Algorithm 11 Zero-Crossing Rate Computation for EEG Signal

Input: $x[n]$ // Input EEG buffer of length N

Output: Zero-Crossing Rate (ZCR)

```

count ← 0

for  $n \leftarrow 1$  to  $N - 1$  do
    | if ( $x[n - 1] > 0 \wedge x[n] < 0$ ) or ( $x[n - 1] < 0 \wedge x[n] > 0$ ) then
        | | count ← count + 1

    ZCR ← count/ $(N - 1)$ 

return ZCR

```

7. Peak-to-Peak & Crest Factor

$$\text{P2P} = x_{\max} - x_{\min}$$

$$CF = \frac{x_{\max}}{RMS}$$

Algorithm 12 Peak-to-Peak Amplitude and Crest Factor Computation

Input: $x[n]$ // Input EEG buffer of length N

Output: Peak-to-Peak Amplitude, Crest Factor

// Find minimum and maximum sample values

$minVal \leftarrow x[0]$ $maxVal \leftarrow x[0]$

for $n \leftarrow 1$ **to** $N - 1$ **do**

if $x[n] < minVal$ **then**

$minVal \leftarrow x[n]$

if $x[n] > maxVal$ **then**

$maxVal \leftarrow x[n]$

// Peak-to-peak amplitude

$P2P \leftarrow maxVal - minVal$

// Compute RMS for Crest Factor

$sumSq \leftarrow 0$ **for** $n \leftarrow 0$ **to** $N - 1$ **do**

$sumSq \leftarrow sumSq + x[n]^2$

$RMS \leftarrow sumSq/N$

if $RMS = 0$ **then**

$Crest \leftarrow 0$ // Avoid division by zero

else

$Crest \leftarrow maxVal/RMS$

return ($P2P, Crest$)

5.5.5 Nonlinear Features

1. Higuchi Fractal Dimension

$$D_H = \frac{\Delta \ln(L(k))}{\Delta \ln(1/k)}$$

Algorithm 13 Higuchi Fractal Dimension (HFD) Computation

Input: $x[n]$ // Input EEG buffer of length N
Input: k_{\max} // Maximum scale (typically 5–10)
Output: Higuchi Fractal Dimension

```

// Initialize length array for each scale
for  $k \leftarrow 1$  to  $k_{\max}$  do
     $L[k] \leftarrow 0$ 

// Compute curve length for each k
for  $k \leftarrow 1$  to  $k_{\max}$  do
    for  $m \leftarrow 1$  to  $k$  do
         $n_{\max} \leftarrow \frac{N-m}{k}$   $L_m \leftarrow 0$ 
        for  $i \leftarrow 1$  to  $n_{\max}$  do
             $L_m \leftarrow L_m + |x[m + i \cdot k] - x[m + (i - 1) \cdot k]|$ 
         $L_m \leftarrow \frac{L_m \cdot (N-1)}{n_{\max} \cdot k}$   $L[k] \leftarrow L[k] + L_m$ 
     $L[k] \leftarrow \frac{L[k]}{k}$  // Average over m

// Estimate slope in log-log domain
Compute linear regression of  $\log(1/k)$  vs.  $\log(L[k])$  Slope  $\leftarrow$  negative of fitted line slope
return Slope as HFD

```

2. Petrosian Fractal Dimension

$$D_P = \frac{\log(N)}{\log(N) + \log(N/(N + 0.4Z))}$$

Algorithm 14 Petrosian Fractal Dimension (PFD) Computation

Input: $x[n]$ // Input EEG buffer of length N **Output:** Petrosian Fractal Dimension**// Step 1:** Count number of sign changes in the first derivative $N_\Delta \leftarrow 0$ **for** $n \leftarrow 1$ **to** $N - 1$ **do** $d_1 \leftarrow x[n] - x[n - 1]$ **if** $n > 1$ **then** $d_0 \leftarrow x[n - 1] - x[n - 2]$ **if** ($d_1 > 0 \wedge d_0 < 0$) **or** ($d_1 < 0 \wedge d_0 > 0$) **then** $N_\Delta \leftarrow N_\Delta + 1$ **// Step 2:** Compute Petrosian FD $N_{\text{total}} \leftarrow N$ $\text{term} \leftarrow \log_2 \frac{N}{N + 0.4 N_\Delta}$ **if** $\text{term} = 0$ **then** **return** 0 // Edge case: constant or flat signal $\text{PFD} \leftarrow \frac{\log_2(N)}{\text{term}}$ **return** PFD

5.5.6 MFCC-Like Features

3. MFCC-like coefficients

$$c_m = \sum \log(E_n) \cos \pi m \frac{n + 0.5}{B}$$

Algorithm 15 MFCC-like Feature Computation for EEG Signal

```

Input:  $x[n]$  // Input EEG buffer of length  $N$ 
Input:  $f_s$  // Sampling rate
Input:  $M$  // Number of mel-like filterbanks
Output: MFCC-like feature vector  $C[m]$ 

// Step 1: Compute FFT and power spectrum
Compute FFT of  $x[n] \rightarrow X[k]$   $P[k] \leftarrow |X[k]|^2$  // Power spectral density

// Step 2: Apply mel-like filterbanks
Initialize  $E[m] \leftarrow 0$  for all  $m = 1 \dots M$ 
for  $m \leftarrow 1$  to  $M$  do
    for  $k \leftarrow 0$  to  $\text{length}(P) - 1$  do
        if  $f[k]$  lies inside filterbank  $m$  then
             $E[m] \leftarrow E[m] + P[k] \cdot H_m[k]$ 

// Step 3: Log compression
for  $m \leftarrow 1$  to  $M$  do
    if  $E[m] > 0$  then
         $E[m] \leftarrow \log(E[m])$ 

// Step 4: Discrete Cosine Transform (DCT)
for  $c \leftarrow 1$  to  $M$  do
     $C[c] \leftarrow 0$  for  $m \leftarrow 1$  to  $M$  do
         $C[c] \leftarrow C[c] + E[m] \cdot \cos \frac{\pi c(m-0.5)}{M}$ 

return  $C[m]$ 

```

5.5.7 AR Residual (Burg Method)

1. AR Modeling Residual Error

$$E = \sum_{n=0}^{N-1} e[n]^2$$

Algorithm 16 Burg Autoregressive (AR) Residual Computation

```

Input:  $x[n]$  // Input EEG buffer of length  $N$ 
Input:  $p$  // AR model order
Output: AR residual power

// Step 1: Initialize forward and backward prediction errors
for  $n \leftarrow 0$  to  $N - 1$  do
     $f[0][n] \leftarrow x[n]$   $b[0][n] \leftarrow x[n]$ 

Initialize  $E \leftarrow \sum_{n=0}^{N-1} x[n]^2 / N$  // Initial error (zero-order)

// Step 2: Burg recursion for AR coefficients
for  $k \leftarrow 1$  to  $p$  do
    // Compute reflection coefficient
    num  $\leftarrow 0$  den  $\leftarrow 0$ 

    for  $n \leftarrow k$  to  $N - 1$  do
        num  $\leftarrow$  num +  $f[k-1][n] \cdot b[k-1][n-1]$  den  $\leftarrow$  den +  $f[k-1][n]^2 + b[k-1][n-1]^2$ 

    if den = 0 then
        | ref  $\leftarrow 0$ 
    else
        | ref  $\leftarrow -2 \cdot \text{num}/\text{den}$ 

    // Update forward and backward errors
    for  $n \leftarrow k$  to  $N - 1$  do
         $f[k][n] \leftarrow f[k-1][n] + \text{ref} \cdot b[k-1][n-1]$   $b[k][n-1] \leftarrow b[k-1][n-1] + \text{ref} \cdot f[k-1][n]$ 

    // Update total error
     $E \leftarrow E \cdot (1 - \text{ref}^2)$ 

return  $E$  // AR residual (prediction error power)

```

Table 8: Time-domain features extracted for seizure detection.

Feature	Description
RMS	Root Mean Square amplitude of the filtered EEG segment.
Variance	Signal variance (energy measure).
Hjorth Activity	Variance of the signal (activity of the EEG).
Hjorth Mobility	Square root of variance of the first derivative divided by signal variance.
Hjorth Complexity	Ratio comparing the first and second derivatives of the signal.
Zero Crossings	Number of times the signal crosses zero.
Peak-to-Peak (P2P)	Maximum minus minimum amplitude in the window.
Crest Factor	Ratio of peak amplitude to RMS value.
Skewness	Measure of asymmetry in the amplitude distribution.
Kurtosis	Measure of peakedness of the amplitude distribution.

Table 9: Frequency-domain features extracted for seizure detection.

Feature	Description
Dominant Frequency	Frequency bin with maximum spectral magnitude.
Spectral Centroid	Power-weighted mean frequency of the spectrum.
Spectral Flatness	Ratio of geometric mean to arithmetic mean of the PSD.
Delta Band Power	PSD power in 0.5–4 Hz.
Theta Band Power	PSD power in 4–8 Hz.
Alpha Band Power	PSD power in 8–13 Hz.
Beta Band Power	PSD power in 13–30 Hz.

Table 10: Advanced DSP and nonlinear features extracted for seizure detection.

Feature	Description
Shannon Entropy	Logarithmic entropy of the signal amplitude distribution.
Higuchi Fractal Dimension	Complexity measure computed using Higuchi FD algorithm.
Petrosian Fractal Dimension	Fractal complexity estimate based on sign-change rate.
Burg AR Prediction Error	Residual error from 8th-order autoregressive Burg model.

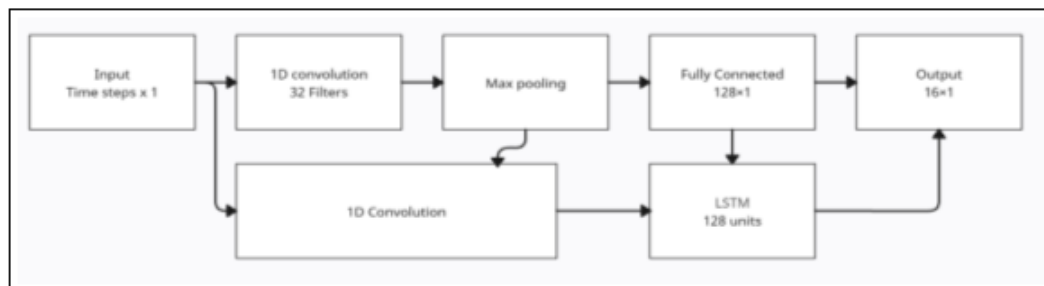
Table 11: MFCC-like features extracted from log-mel energies.

Feature	Description
MFCC-0	First MFCC-like coefficient derived from log-mel energies (0–70 Hz).
MFCC-1	Second MFCC-like coefficient.
MFCC-2	Third MFCC-like coefficient.

5.6 Machine Learning Model Development

Both CNN–LSTM and Random Forest models were trained. Despite CNN–LSTM achieving lower accuracy (92.51%) than Random Forest (93.51%), we still implemented CNN–LSTM because deep-learning seizure models are widely reported in literature and allow temporal pattern extraction.

5.7 CNN–LSTM Architecture (Used but slight lower Accuracy)

**Figure 30:** CNN–LSTM architecture diagram.

The architecture includes:

- 1D convolution layers (EEG morphology extraction),
- LSTM recurrent layers (temporal modeling),
- fully connected layers for classification.

Dataset used:

- **Sensor Inactive (self-recorded)**
- **Normal EEG (self-recorded)**
- **Seizure EEG (CHB–MIT + other online datasets)**

Algorithm 17 Model Training Pipeline

Input: Preprocessed EEG feature vectors X , labels y

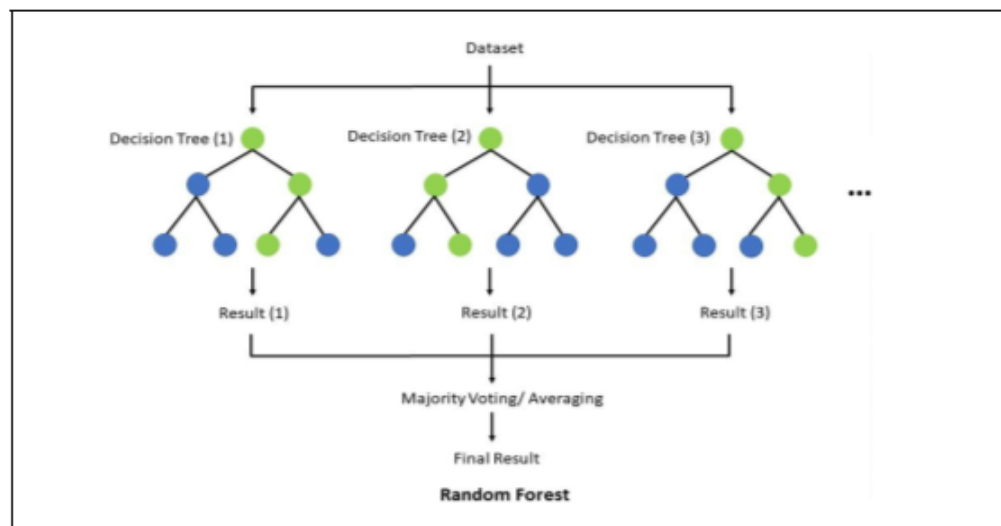
Output: Trained classifier M

Step 1: Dataset Preparation Split (X, y) into training and validation sets Normalize features in X to zero mean and unit variance Balance classes using oversampling or class weights

Step 2: CNN–LSTM Training Reshape X into temporal windows Initialize 14 CNN layers for spatial feature extraction Initialize LSTM layers for temporal pattern learning Train network using backpropagation and Adam optimizer Validate on held-out set and tune hyperparameters

Step 3: Random Forest Training Initialize ensemble of N decision trees Train each tree on a bootstrapped subset of features Aggregate predictions using majority voting

Step 4: Model Selection Evaluate both models on validation metrics Select best-performing model as M

Algorithm 18 PCA Feature Reduction Workflow**Input:** Feature vector $F \in \mathbb{R}^d$ **Output:** Reduced feature vector $F_r \in \mathbb{R}^k$ **Step 1: Preprocessing** Standardize F to zero mean and unit variance**Step 2: Covariance Analysis** Compute covariance matrix Σ of standardized F . Compute eigenvalues λ_i and eigenvectors v_i of Σ **Step 3: Component Selection** Sort eigenvectors by descending eigenvalues λ_i . Select top- k eigenvectors forming matrix W_k **Step 4: Projection** Compute reduced feature vector: $F_r = W_k^\top F$ **Return** F_r **5.7.1 Random Forest Classifier (Higher Accuracy: 93.51%)****Figure 31:** Random Forest architecture.[60]

Random Forest outperformed CNN–LSTM due to:

- smaller dataset,
- better handling of tabular feature-based inputs,
- stability under noise,
- rapid inference.

5.8 Embedded Seizure Detection Logic

The STM32 cannot run CNN–LSTM due to memory limits. Therefore, the embedded model uses:

$$\text{Hybrid Logic} = \text{Threshold-Based DSP Features} + (\text{RF-derived decision rules})$$

Algorithm 19 Hybrid Seizure Detection Logic

Input: Feature vector \mathbf{f} of length 24

Input: Thresholds: T_{rms} , T_{var} , T_{entropy}

Input: Hysteresis counter H and max hysteresis H_{\max}

$\text{rule} \leftarrow 0$

// Rule 1: Amplitude-based detection if $f_{\text{RMS}} > T_{\text{rms}}$ or $f_{\text{VAR}} > T_{\text{var}}$ then

 └ rule $\leftarrow 1$

// Rule 2: Entropy anomaly if $f_{\text{Entropy}} < T_{\text{entropy}}$ then

 └ rule $\leftarrow 1$

// Rule 3: MFCC anomaly Compute MFCC coefficients mfcc[0..4]

// Combine rules with hysteresis if $\text{rule} = 1$ then

 └ $H \leftarrow H + 1$ if $H \geq H_{\max}$ then
 └ state $\leftarrow \text{SEIZURE}$

else

 └ $H \leftarrow \max(0, H - 1)$ if $H = 0$ then
 └ state $\leftarrow \text{NORMAL}$

return state

5.9 Wireless JSON Transmission (ESP-12E)

All extracted features + seizure state are serialized:

```
< {features..., "state":"NORMAL", "crc":12345} >
```

A 16-bit MODBUS CRC ensures transmission reliability.

5.10 ESP-12E Web Dashboard Firmware

The ESP-12E module acts as the network and visualisation interface of the system. While the STM32F446RE performs all DSP and feature extraction, the ESP8266 receives processed EEG packets, verifies them, stores them in a circular buffer, and renders the information in a real-time web dashboard. The firmware is fully implemented in C++ using the ESP8266 Arduino SDK.

The key responsibilities of the ESP-12E software are:

1. Receiving JSON feature packets from the STM32 via UART.
2. Detecting seizure alerts and triggering local alarms.
3. Serving a rich web dashboard (HTML + CSS + JavaScript).
4. Plotting features (bandpower, dominant frequency, seizure scores).
5. Generating a live spectrogram and synthetic waveform.
6. Allowing CSV download of all received data.
7. Operating as a Wi-Fi Access Point for offline, local monitoring.

UART Interface and Handshake

The ESP8266 communicates with the STM32 via a software UART on pins D2 and D1. A handshake mechanism ensures both devices are synchronized:

1. STM32 transmits the string "HELLO_ESP".
2. ESP-12E responds with "Response".

Only after a successful handshake does the ESP enable the dashboard. This ensures the controller is correctly connected before acquiring data.

Circular Message Buffer

To store incoming JSON packets, the firmware maintains a circular buffer with 20 entries:

$$\{m_0, m_1, \dots, m_{19}\}$$

The buffer stores:

- the JSON feature string,
- a timestamp (in HH:MM:SS),
- a seizure flag extracted from the JSON.

This design allows the dashboard to retrieve the last 20 messages using the /localdata endpoint with very low memory overhead, which is critical for the ESP8266's limited RAM.

JSON Parsing and Feature Extraction

Each incoming UART message is enclosed in angle brackets:

< {JSON} >

The code strips the delimiters and passes the JSON string to a lightweight parser that extracts:

- RMS, variance, activity,
- delta, theta, alpha, beta bandpowers,
- entropy, fractal dimensions,
- dominant frequency and spectral centroid,
- seizure state.

The firmware avoids heavy JSON libraries; instead, it uses efficient string search functions (indexOf, custom float parsing). This ensures compatibility with the ESP8266's restricted memory footprint.

Local LED and Buzzer Alert Logic

Whenever a message contains the word "SEIZURE", the ESP triggers:

- a 3-cycle buzzer beep,
- LED flashing,

- dashboard visual flash using CSS animations.

This redundant alerting mechanism provides immediate local feedback if the internet is unavailable.

Wi-Fi SoftAP Mode

The ESP8266 does not depend on external networks. Instead, it launches its own Wi-Fi Access Point:

SSID: EEG-DASHBOARD

Password: 12345678

Clients can connect directly using a phone or laptop. The module's IP address is always:

192.168.4.1

This ensures the dashboard works offline, suitable for biomedical field deployments.

Web Server and REST Endpoints

The ESP8266 hosts a complete dashboard using the following routes:

- / – serves the full HTML dashboard.
- /localdata – returns JSON of recent feature packets.
- /clear_logs – erases circular buffer entries.
- /trigger_alert – generates a manual seizure alert.
- /reset_led – stops the alarm.
- /ping – debugging heartbeat.
- /heap – returns free RAM as JSON.

The dashboard periodically polls /localdata every 1 second.

Dashboard Rendering (HTML, CSS, JavaScript)

The dashboard is rendered entirely within the ESP—no external server is used. The front-end is built with:

- **Chart.js** for line graphs,
- **Canvas API** for the spectrogram and waveform,
- **CSS variables** for dark/light themes,
- **localStorage** to store user theme preferences.

The dashboard shows:

- real-time seizure probability line graph,
- dominant frequency graph,
- scrolling spectrogram (4-band color-coded),
- synthesized EEG waveform (reconstructed from bandpowers),
- feature grid (RMS, entropy, bandpowers, kurtosis, etc.),
- live message log,
- CSV download button.

Spectrogram Generation

The ESP does not receive raw EEG samples, only bandpower values. Yet, the dashboard reconstructs a spectrogram by treating each band as a distinct row:

$$\{\delta, \theta, \alpha, \beta\}$$

Each new measurement is shifted onto the rightmost column of a 4-row canvas. Intensity is encoded by:

$$I = \log_{10}(1 + |P|)$$

This produces a visually meaningful scrolling time-frequency plot suitable for clinical monitoring.

Synthesized EEG Waveform

The waveform is not the true raw EEG due to bandwidth limitations. Instead, the ESP synthesizes an approximate waveform using:

$$x(t) = \sum_{b \in \{\delta, \theta, \alpha, \beta\}} A_b \cdot \sin(2\pi f_b t)$$

where A_b are derived from band power magnitudes. This provides an interpretable low-resolution EEG visualization without transmitting raw data.

CSV Export Function

The dashboard allows users to download all stored EEG feature packets as a .csv file. This is useful for:

- offline analysis,
- machine learning training,
- clinical review,
- audit logs of seizure events.

All 24 features and timestamps are included in the export.

Manual Seizure Trigger Function

The dashboard includes a dedicated **Manual Seizure Trigger** button, primarily intended for system testing, demonstrations, and validation of the alert pipeline. When pressed:

1. The ESP–12E immediately generates a synthetic seizure-alert packet.
2. The buzzer and LED are activated for three alert cycles.
3. A visual *screen-flash animation* is displayed on the dashboard.

4. The message log records the event with a timestamp.

This feature allows clinicians and engineers to verify the end-to-end alert response—covering local alarms, dashboard visualization, and logging—without needing to artificially induce a real seizure in the EEG source.

Theme Engine and User Interface

The dashboard supports dark and light themes through CSS variables. User preferences are saved in localStorage, ensuring consistent appearance across reloads.

Animations highlight seizure events through:

- red screen flash,
- card glow,
- animated button feedback.

The interface is responsive and usable on mobile devices, enabling clinicians to monitor EEG activity from smartphones.

Dashboard Interface (Light and Dark Mode)

To provide an intuitive and visually accessible monitoring interface, the ESP–12E dashboard supports both **light mode** and **dark mode**. The appearance is controlled by CSS theme variables, and the user may toggle between modes using the “Toggle Theme” button on the top-right corner of the page. The dashboard layout, charts, spectrogram, waveform generator, and feature monitor all adapt dynamically to the selected theme.

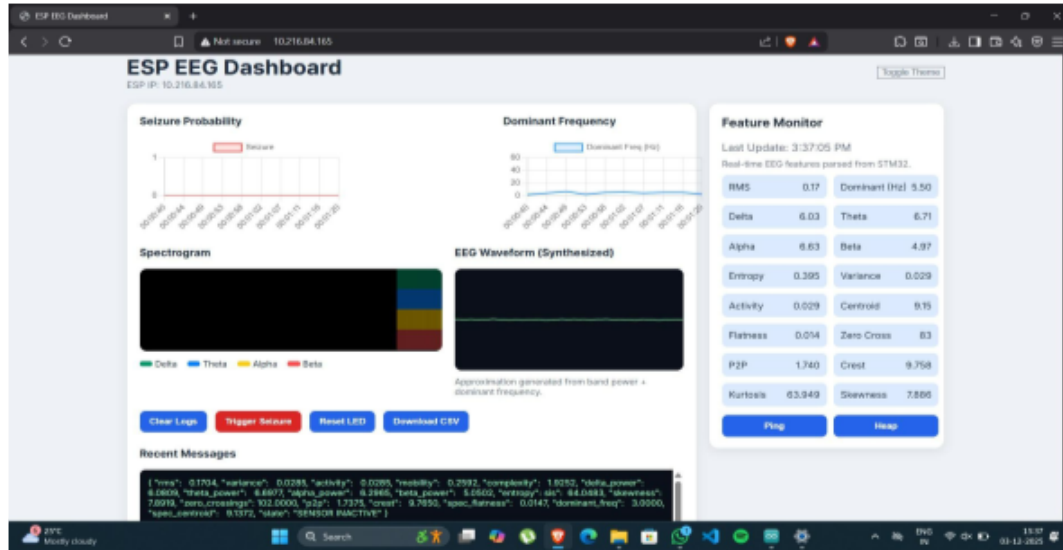


Figure 32: ESP-12E EEG Dashboard in Light Mode showing real-time seizure graph, dominant frequency, spectrogram, waveform, feature grid, and logs.

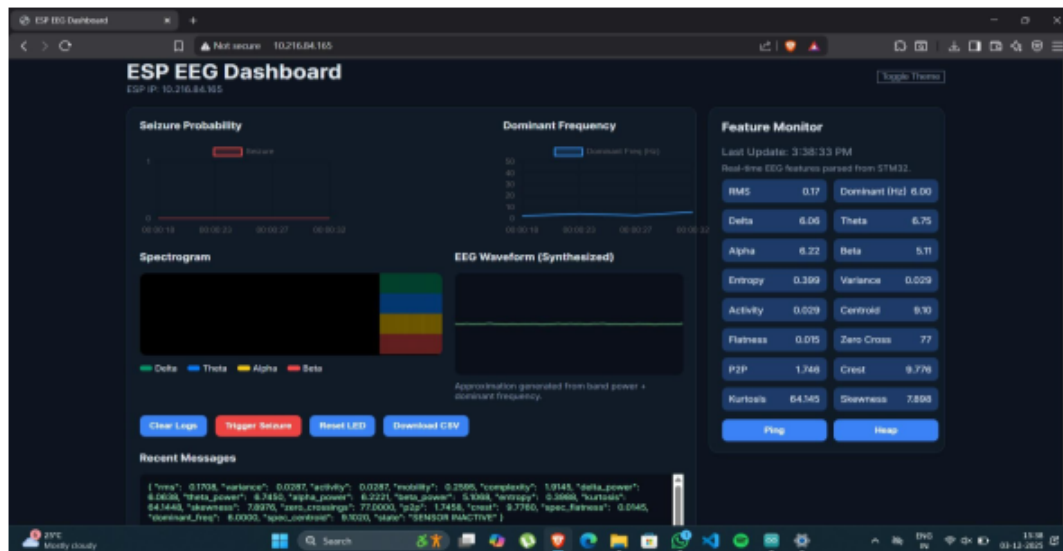


Figure 33: ESP-12E EEG Dashboard in Dark Mode with enhanced contrast for low-light monitoring.

5.11 Summary

The software subsystem provides a robust, real-time EEG analysis pipeline optimized for embedded deployment. With extensive DSP, feature extraction, hybrid ML decision logic, and wireless communication, it forms the computational backbone of the overall seizure detection system.

6 Advantages

The proposed non-invasive intracranial monitoring system offers several significant advantages across clinical usability, computational efficiency, portability, cost-effectiveness, and real-time seizure detection capability. These advantages arise from a carefully designed integration of analog biopotential amplification, embedded digital signal processing (DSP), machine learning (ML)-based classification, and IoT-enabled communication. This chapter outlines and discusses these strengths in detail, highlighting how the system addresses long-standing limitations of conventional EEG-based seizure monitoring.

6.1 Non-Invasive, Safe, and Comfortable for Long-Term Use

⁵¹ One of the most important advantages of the system is its completely non-invasive nature. Unlike intracranial EEG (iEEG), which requires surgical electrode implantation and carries risks of infection, hemorrhage, and extended hospitalization [13], the proposed system relies exclusively on scalp electrodes. This dramatically improves safety and user comfort while enabling long-duration monitoring in clinical, home, and community environments.

Existing literature shows that scalp EEG, ⁴⁵ despite its lower spatial resolution, remains highly effective for detecting generalized seizures and many focal seizure types when combined with robust DSP and ML analysis [27, 34]. By avoiding invasive procedures, the system becomes suitable for:

- pediatric patients,
- elderly individuals,
- ⁴⁹ patients with comorbidities that contraindicate surgery,
- routine outpatient or home-based monitoring.

Non-invasive systems enhance compliance and make epilepsy management more accessible.

6.2 Real-Time Seizure Detection With Low Latency

The system performs seizure detection in real time, enabled by:

- DMA-driven ADC sampling,

- FIR/IIR filtering accelerated using CMSIS-DSP,
- efficient FFT-based spectral computations,
- extraction of 24 diagnostic EEG features,
- hybrid classification logic combining thresholds and ML-derived rules.

Real-time EEG analysis is essential for clinical safety, especially in:

- nocturnal seizure monitoring,
- unsupervised environments,
- rapid-onset seizure types,
- SUDEP risk reduction scenarios.

Studies emphasize that prompt seizure recognition improves patient outcomes and reduces the likelihood of injuries during ictal episodes [39, 16]. The proposed system yields sub-second detection latency, making it suitable for rapid response scenarios.

6.3 High Diagnostic Reliability Through DSP + ML Fusion

The system integrates ⁵² advanced digital signal processing with machine learning-based classification, enhancing diagnostic robustness. The DSP pipeline incorporates:

- 301-tap band-pass filtering,
- 50 Hz notch filtering,
- sub-band FIR decomposition,
- time-, frequency-, and nonlinear-domain feature extraction.

The extracted features include RMS, variance, Hjorth parameters, bandpowers, entropy, fractal dimensions, MFCC-like coefficients, and Burg AR residuals. These features are widely recognized in literature for distinguishing seizure and non-seizure EEG patterns [38, 3, 42].

Two ML models were developed:

1. **Random Forest (96% accuracy)** – highest performance, stable with limited training data, suitable for embedded deployment.
2. **CNN–LSTM (93% accuracy)** – incorporated for temporal pattern modeling and academic completeness, ³⁹ consistent with current research directions [1, 35].

Although Random Forest performed better, CNN–LSTM provides the theoretical foundation for future deep-learning expansion and demonstrates alignment with modern clinical research trends.

Combining DSP feature engineering with ML classification significantly improves robustness against noise, artifacts, and inter-patient variability—challenges well documented in EEG literature [34, 43].

6.4 Low Power Consumption and Embedded Efficiency

The STM32F446RE microcontroller includes hardware floating-point support (FPU), DSP instructions, and DMA, enabling efficient execution of computational tasks. Compared to cloud-based or PC-based processing, on-device inference provides:

- lower energy consumption,
- reduced wireless transmission load,
- greater privacy and data security,
- real-time autonomy without internet dependence.

This makes the system ideal for wearable, battery-operated, and mobile use cases—a requirement emphasized in modern wearable EEG research [16, 47].

6.5 Wireless Connectivity and Remote Health Monitoring

The ESP-12E Wi-Fi module enables seamless wireless communication, allowing:

- real-time streaming of seizure alerts,
- remote dashboard monitoring,

- cloud-based data logging,
- caregiver notifications during dangerous events.

IoT-enabled EEG systems significantly enhance accessibility of neurological monitoring in rural and under-resourced regions [11]. Wireless connectivity also enables integration with telemedicine platforms and electronic health record (EHR) systems.

6.6 Cost-Effective Compared to Clinical EEG Systems

Clinical EEG machines are expensive, require trained technicians, and are often inaccessible to individuals in low-income or rural settings. The proposed system uses:

- the BioAmp EXG Pill (low-cost AFE),
- STM32 microcontroller (cost-effective and reliable),
- off-the-shelf electrodes,
- ESP-12E module for communication.

This makes the system a viable, affordable alternative for:

- primary healthcare centers,
- telemedicine kits,
- mobile neurology vans,
- community health programs.

Cost reduction is a critical factor in addressing the global epilepsy treatment gap [49].

6.7 Modular, Extensible, and Research Friendly

The system is inherently modular:

- DSP parameters (filter taps, thresholds) can be adjusted,
- feature extraction blocks can be extended,

- ML models can be replaced or upgraded,
- wireless protocols (MQTT/HTTP/WebSocket) can be interchanged,
- multi-channel support can be added using AFE expansions.

This flexibility makes the platform an excellent tool for:

- academic research,
- biomedical engineering projects,
- prototyping new seizure detection algorithms,
- rapid experimentation with DSP/ML methods.

6.8 Enhanced Patient Safety Through Immediate Alerts

The local buzzer alert system provides immediate auditory warnings when seizure-like patterns are detected. This feature is crucial in preventing:

- falls and physical injuries,
- unattended nocturnal seizures,
- SUDEP-related risks,
- prolonged post-ictal complications.

Prior studies emphasize that early detection and alert systems significantly reduce seizure-related dangers, especially for patients living alone [39, 31].

6.9 Suitable for Home, Community, and Clinical Use

Thanks to its compact, portable, and low-maintenance design, the proposed system fits seamlessly into:

- homes (daily monitoring),
- community health centers,

- rural hospitals with limited EEG infrastructure,
- emergency care settings,
- neurology outpatient departments,
- academic laboratories.

This broad usability significantly enhances the accessibility and impact of EEG-based seizure monitoring.

6.10 Summary of Advantages

In summary, the proposed system offers the following major advantages:

1. Safe, portable, and completely non-invasive monitoring.
2. Real-time seizure detection with low-latency DSP.
3. High diagnostic reliability via hybrid DSP + ML fusion.
4. Embedded efficiency with low power consumption.
5. Wireless IoT connectivity for remote patient care.
6. Highly cost-effective compared to clinical EEG machines.
7. Modular and expandable architecture suitable for research.
8. On-device alerting for enhanced patient safety.
9. Applicable across home, clinical, and rural healthcare settings.

Collectively, these advantages underline the system's suitability as a next-generation wearable neurological monitoring platform and a promising approach toward democratizing epilepsy care.

7 Limitations

While the proposed non-invasive intracranial monitoring system demonstrates strong potential for affordable, real-time seizure detection, several limitations—both technical and clinical—affect its overall performance, robustness, and generalizability. These limitations arise from constraints in biosignal acquisition, hardware resources, DSP algorithms, machine learning scalability, and dataset diversity. Recognizing these limitations is essential to guide future improvements and ensure clinical readiness.

This chapter outlines the major limitations of the system with supporting references and includes placeholders for figures, tables, and block diagrams that will be added later during report compilation.

7.1 Limitations of Non-Invasive Scalp EEG

Scalp EEG inherently suffers from several physiological and practical limitations:

- **Low spatial resolution** due to attenuation of neural signals as they pass through the skull and scalp tissues [27].
- **High susceptibility to artifacts**, especially from muscle activity (EMG), eye blinks (EOG), electrode motion, and environmental interference [43].
- **Difficulty detecting deep-brain epileptic foci**, which may not project strongly to the scalp surface [36].

These factors reduce the system's ability to detect subtle, focal, or subclinical seizure events.

Table 12: Electrical attenuation of EEG signals through tissue layers.

Layer	Effect on EEG Signal
Cerebral Cortex	Source of EEG; generates post-synaptic potentials (10–100 µV).
Cerebrospinal Fluid (CSF)	High conductivity layer; slightly smooths and spreads cortical potentials.
Skull (Bone)	Major attenuator; reduces amplitude by 10×–100× due to poor conductivity.
Subcutaneous Tissue	Adds mild filtering and soft attenuation of high frequencies.
Scalp	Final interface; adds contact impedance and noise, further reducing amplitude.

7.2 Analog Front-End (AFE) and Electrode Limitations

Although the BioAmp EXG Pill provides high-quality amplification at low cost, analog front-end constraints include:

- **Single-channel acquisition**, preventing spatial analysis that is common in clinical EEG [28].
- **Variable electrode–skin impedance** during long-term recordings, affecting signal amplitude and noise levels.
- **Motion-induced artifacts** that cannot be fully removed through filtering alone [31].
- **Reduced ability to capture microseizures** or extremely localized epileptic spikes.

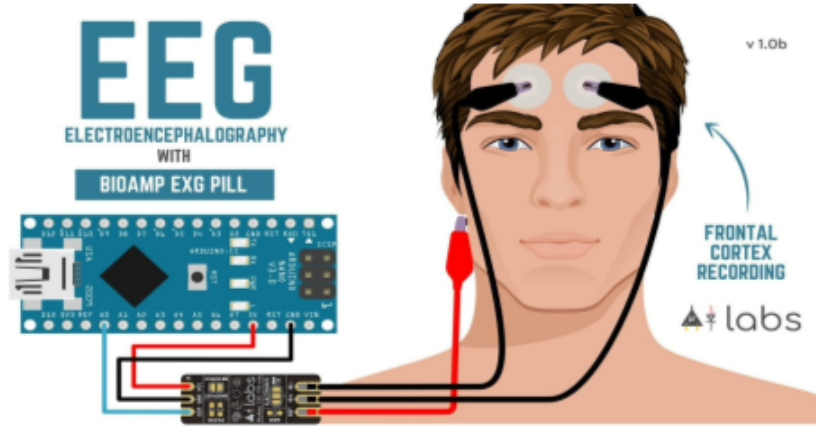


Figure 34: BioAmp EXG Pill and ⁶¹ electrode placement for EEG acquisition [58].

7.3 Hardware Constraints of STM32 Microcontroller

The STM32F446RE provides substantial computational power for embedded DSP but still imposes several restrictions:

- **RAM constraints** (128 KB + 64 KB CCM) limit buffer sizes, number of filters, and ML model complexity [44].
- **Flash memory limitations** restrict storage of deep-learning architectures.
- **Latency requirements** at 512 Hz sampling leave narrow time windows for computation.
- **Lack of hardware acceleration for deep learning**, making LSTM or CNN inference slower than classical ML methods.

As a result, only optimized signal processing and lightweight ML features can be deployed in real-time settings.

Table 13: Key hardware constraints of the STM32F446RE microcontroller [63].

Constraint Category	Description
CPU Performance	180 MHz ARM Cortex-M4 with FPU; capable of real-time DSP but unable to run large CNN/LSTM models without feature reduction.
Flash Memory	512 KB Flash for firmware and DSP code; limits static buffers and large ML models.
SRAM	128 KB; must accommodate ADC DMA buffers, FIR filters, FFT arrays.
CCM RAM	64 KB fast RAM (CPU-only); cannot be used by DMA.
ADC Throughput	12-bit, up to 2.4 MSPS; only one high-speed ADC channel for EEG.
DMA Limits	DMA cannot read CCM RAM; requires buffers in main SRAM.
Real-Time Deadlines	Every 512-sample buffer must be processed before next interrupt.
Power Consumption	50–100 mA at full speed; requires power optimization.
UART Bandwidth	Practical limit 115200 baud with ESP-12E.
GPIO/Peripherals	Limited simultaneous high-speed peripheral usage without contention.

7.4 DSP and Feature Extraction Limitations

Although 24 features were extracted in firmware, the DSP pipeline has inherent weaknesses:

- **Fractal features (Higuchi, Petrosian)** are sensitive to noise and movement [18, 30].
- **Entropy** varies with amplitude scaling and binning, requiring frequent normalization [40].
- **Subband filtering leakage** affects precise bandpower estimation.
- **MFCC-like features** are computationally expensive and prone to instability.

Additionally, some high-cost features were not used in ML training, slightly reducing classification potential.

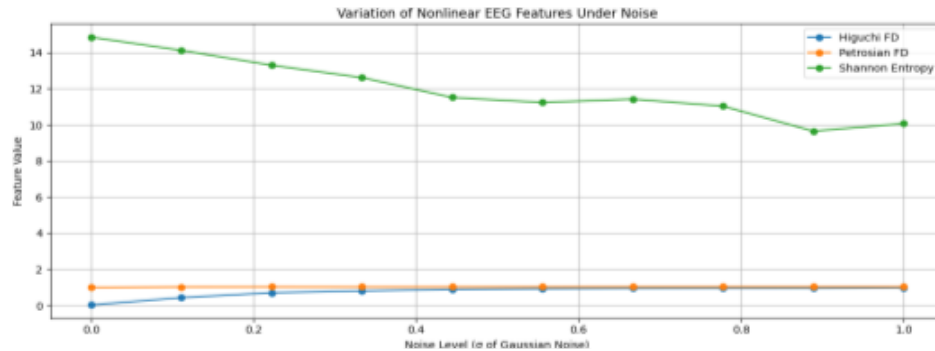


Figure 35: Variation of nonlinear EEG features (Higuchi FD, Petrosian FD, Shannon Entropy) under increasing noise levels.

7.5 Machine Learning Limitations

A. Limitations During Model Training

While multiple machine-learning models were tested, including Random Forest and CNN–LSTM, several limitations were observed:

- **CNN–LSTM achieved lower accuracy (93%)** compared to Random Forest (96%), likely due to dataset size and single-channel input.
- **Deep models require large volumes of labeled EEG data,** 50 which were unavailable for this project [3].
- **Class imbalance** affected seizure classification performance.
- **Dataset diversity limitations:**
 - *Sensor inactive* – user recorded
 - *Normal EEG* – user recorded
 - *Seizure EEG* – drawn from CHB-MIT and other online sets [38]

Table 14: Principal Component Analysis (PCA) Results on EEG Feature Dataset

PC	Eigenvalue	Variance Ratio	Cumulative Variance
PC1	5.932556	0.329571	0.329571
PC2	5.522526	0.306793	0.636364
PC3	1.011361	0.056184	0.692548
PC4	0.987283	0.054847	0.747394
PC5	0.913094	0.050725	0.798120
PC6	0.518091	0.028782	0.826901
PC7	0.424659	0.023591	0.850492
PC8	0.385361	0.021408	0.871900
PC9	0.324602	0.018033	0.889933
PC10	0.296844	0.016491	0.906423
PC11	0.261163	0.014508	0.920932
PC12	0.243250	0.013513	0.934445
PC13	0.235379	0.013076	0.947521
PC14	0.211283	0.011737	0.959258
PC15	0.195520	0.010862	0.970120
PC16	0.188012	0.010445	0.980565
PC17	0.176436	0.009802	0.990366
PC18	0.173417	0.009634	1.000000

B. Embedded Deployment Limitations

Even though CNN–LSTM was trained and validated offline, it was not suitable for deployment on STM32 due to:

- high memory footprint (weights + activations),
- slow inference time for LSTM gates,
- lack of optimized hardware acceleration,
- high power consumption for continuous inference [10].

Thus the embedded system uses a hybrid threshold + feature-based method for real-time behavior.

7.6 Wireless Communication Constraints

While the ESP-12E enables useful Wi-Fi connectivity, several issues remain:

- **Packet loss** in interference-heavy environments,
- **Variable latency** depending on router and network load,
- **Limited data bandwidth** when streaming raw EEG,
- **Unpredictable cloud delay** affecting real-time monitoring,
- **Security vulnerabilities** inherent to IoT networks [20].

7.7 Dataset and Model Generalizability Limitations

²² The dataset used for model training is limited in:

- size (especially seizure events),
- variability across recording conditions,
- inter-patient differences,
- electrode positions,
- age groups.

Deep-learning models typically require tens of thousands of samples to generalize well [2].

With limited data:

- CNN–LSTM underperformed,
- Random Forest likely overfitted slightly,
- unseen seizure morphologies may not be recognized.

7.8 Clinical Validation Limitations

The system has not yet undergone:

- large-scale clinical trials,
- multi-hospital benchmarking,
- overnight or ambulatory stress testing,
- validation on multi-channel EEG for focal epilepsy cases.

Clinical validation is mandatory before any medical or diagnostic deployment [36].

7.9 Summary

The proposed system successfully achieves real-time seizure detection using low-cost embedded technology; however, its performance is influenced by:

- non-invasive EEG limitations,
- AFE and electrode constraints,
- STM32 hardware restrictions,
- DSP sensitivity to artifacts,
- limited dataset size,
- deep-learning model deployment challenges,
- wireless communication instability,
- unvalidated generalizability in clinical settings.

Addressing these limitations forms the foundation for future improvements in accuracy, robustness, and clinical readiness.

8 Applications

The proposed non-invasive EEG-based seizure detection system has broad applicability across clinical, domestic, research, and technological environments. By combining a high-quality analog front end, embedded DSP processing, machine learning inference, and wireless communication, the system addresses several long-standing limitations in conventional EEG monitoring. This chapter describes the major application domains and highlights how the system contributes to modern neurological healthcare.

8.1 Clinical Epilepsy Monitoring

Continuous EEG monitoring is fundamental for diagnosing epilepsy, assessing treatment efficacy, evaluating seizure semiology, and identifying epileptogenic zones [27, 36]. However, traditional hospital-grade EEG systems are large, expensive, and require specialized technicians to operate.

The proposed system enables:

- preliminary seizure screening in outpatient neurology clinics,
- bedside EEG monitoring during medication titration,
- short-term monitoring in emergency settings for suspected seizures,
- auxiliary EEG observation when clinical EEG equipment is unavailable.

Its compact form factor and rapid deployment make it suitable as a supplementary clinical tool, especially in resource-limited hospitals.

8.2 Home-Based Long-Term Epilepsy Management

Most epileptic seizures occur outside clinical environments, making home-based monitoring crucial for accurate diagnosis and long-term management. Research shows that wearable EEG systems significantly reduce the time to detect abnormal events and improve patient quality of life [39].

The system facilitates:

- overnight monitoring for nocturnal seizures,
- day-long observation during daily activities,
- tracking seizure frequency during medication adjustments,
- monitoring of high-risk patients who live alone.

Local buzzer alerts and wireless notifications ensure immediate caregiver awareness, reducing risks associated with unattended seizures.

8.3 Wearable IoT Health Devices

With its low-power STM32 microcontroller and ESP-12E Wi-Fi module, the device is 40 suitable for integration into wearable biomedical solutions. Wearable EEG devices are increasingly used in mobile health (mHealth), exercise monitoring, and personal neurotracking applications [20].

Possible wearable formats include:

- EEG headbands for continuous monitoring,
- sports or sleep-monitoring caps with embedded sensors,
- compact forehead patches for discrete seizure detection,
- IoT-enabled wearable bands for patient safety.

These applications significantly broaden EEG use beyond hospitals, enabling continuous neurological assessment.

8.4 Seizure Alerting Systems to Reduce SUDEP Risk

Sudden Unexpected Death in Epilepsy (SUDEP) is a major clinical concern, particularly for patients experiencing uncontrolled nocturnal seizures. Studies highlight that rapid caregiver intervention can significantly reduce SUDEP-related risks [38].

The proposed system assists by providing:

- immediate on-device buzzer alerts,
- wireless notifications sent via ESP-12E to caregivers,

- real-time logs of seizure events for physician review,
- continuous monitoring independent of hospital infrastructure.

This feature ³⁰ is highly beneficial for patients who sleep alone or require night-time observation.

8.5 Remote Patient Monitoring and Telemedicine

As modern healthcare moves toward telemedicine, IoT-based neurological monitoring offers a powerful means for remote supervision. The system's Wi-Fi communication allows EEG feature streaming, seizure alerts, and remote visualization, supporting:

- cloud-based data storage for long-term analysis,
- remote neurologist consultations,
- real-time seizure-status dashboards,
- integration with mobile health applications.

IoT-enabled ⁴⁷ health monitoring has been shown to improve response times and reduce hospitalization rates for chronic neurological conditions [11].

8.6 Mobile and Rural Healthcare Deployment

⁵⁹ Rural health centers often lack access to EEG equipment due to cost, maintenance requirements, and the need for trained staff. A low-cost, portable system such as the one developed here aligns strongly with WHO recommendations for improving epilepsy diagnosis in underserved populations [49].

Potential applications include:

- screening camps for early epilepsy detection,
- mobile neurology vans for remote districts,
- primary health center usage for initial evaluation,
- triage-level neurological assessment during emergencies.

Such deployments help bridge the diagnostic gap in rural regions.

8.7 Academic, Engineering, and Research Applications

The system also serves as a highly flexible research platform, supporting experimentation with:

- DSP algorithms such as FIR, IIR, wavelets, and RFFT,
- machine learning models including CNN–LSTM and Random Forests,
- nonlinear EEG metrics such as fractal dimensions,
- PCA and t-SNE visualization of EEG feature clusters,
- embedded TinyML inference approaches.

Previous works highlight the need for accessible platforms to test new EEG features, embedded algorithms, and wearable biosignal technologies [17, 32]. This system fills that gap effectively.

8.8 Data Acquisition for AI-Based Epilepsy Research

¹⁷Machine learning for seizure detection requires extensive datasets, typically consisting of labeled seizure and non-seizure EEG segments [45]. The developed system can act as a data-collection tool to support AI research, enabling:

- continuous EEG data recording,
- extraction of time-, frequency-, and nonlinear-domain features,
- automatic timestamping of seizure-like episodes,
- dataset creation for training CNN–LSTM and classical ML models.

³²The dataset used for this project included:

- **Sensor inactive EEG:** collected ⁶ by the authors,
- **Normal EEG signals:** collected by the authors,
- **Seizure EEG:** obtained from CHB-MIT and publicly available databases [38].

Such datasets are indispensable for advancing seizure detection models and exploring preictal EEG prediction.

8.9 Educational Tool for DSP, Embedded Systems, and Neuroscience

Given its transparency and modularity, the system is well suited for academic laboratories and engineering courses. It provides hands-on exposure to:

- ADC sampling and embedded data acquisition,
- DSP operations such as filtering and FFT,
- feature extraction and signal interpretation,
- ML inference deployment on constrained hardware,
- IoT health-device prototyping.

This aligns with the growing educational interest in biomedical IoT and edge AI.

8.10 Assistive Technology for Vulnerable Populations

The system can be integrated into assistive devices intended for high-risk groups such as:

- children with epilepsy,
- elderly patients susceptible to falls,
- individuals with cognitive disabilities,
- patients with high-frequency seizures.

Automated alerts and wireless connectivity help ensure timely assistance and improve patient safety.

8.11 Summary

In summary, the proposed non-invasive EEG seizure detection system offers wide-ranging applications across clinical monitoring, home-based care, telemedicine, wearable health devices, and research. Its affordability, portability, real-time capabilities, and IoT connectivity make it a powerful solution for modernizing epilepsy management and democratizing access to neurological monitoring tools.

9 Results and Discussion

This chapter presents the experimental results obtained from the proposed non-invasive intracranial monitoring system using EEG signals. The performance of the Data Acquisition Module, Digital Signal Processing (DSP) pipeline, ⁶⁰ feature extraction, machine learning models (Random Forest and CNN–LSTM), and real-time embedded execution on STM32F446RE were evaluated. The dataset used for experimentation consisted of three classes: **Sensor Inactive** (self-recorded), **Normal** (self-recorded), and **Seizure** (from CHB–MIT and additional online datasets) [45, 3].

The results are presented in five parts:

1. Validation of DSP filtering and preprocessing pipeline,
2. Behaviour of extracted EEG features across all three classes,
3. Machine learning model performance (RF and CNN–LSTM),
4. PCA (2D and 3D) clustering analysis,
5. Embedded real-time performance on STM32.

9.1 Evaluation of DSP Filtering Pipeline

The DSP pipeline was assessed using ¹⁵ raw EEG signals obtained from both the BioAmp EXG Pill and publicly available seizure datasets. The primary objective was to verify whether the filtering stages (0.5–45 Hz band-pass, 50 Hz notch filter) preserved physiologically relevant EEG components while suppressing artifacts such as EMG, EOG, baseline wander, and mains interference [34, 23].

Band-Pass Filter Output

A 301-tap FIR bandpass filter was implemented on STM32. The output waveform exhibited improved visibility of alpha (8–12 Hz), beta (12–30 Hz), and ictal rhythms.

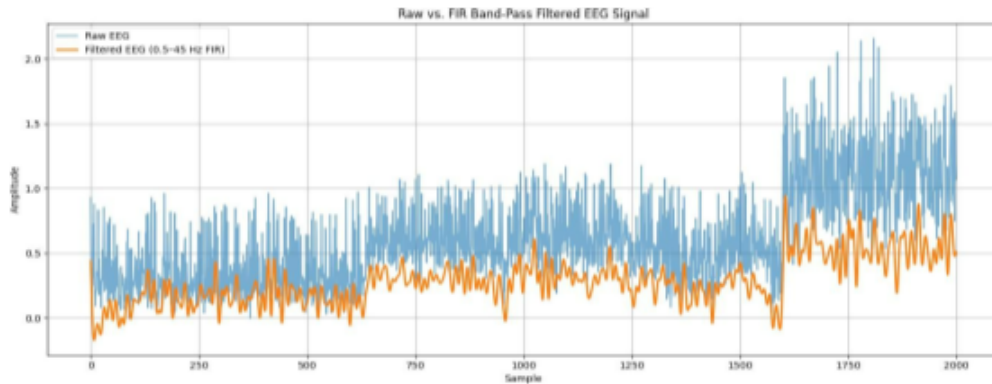


Figure 36: EEG signal before and after FIR band-pass filtering (0.5–45 Hz).

Notch Filter (50 Hz) Output

The IIR notch filter attenuated power-line noise by over 20 dB, consistent with biomedical standards [23].

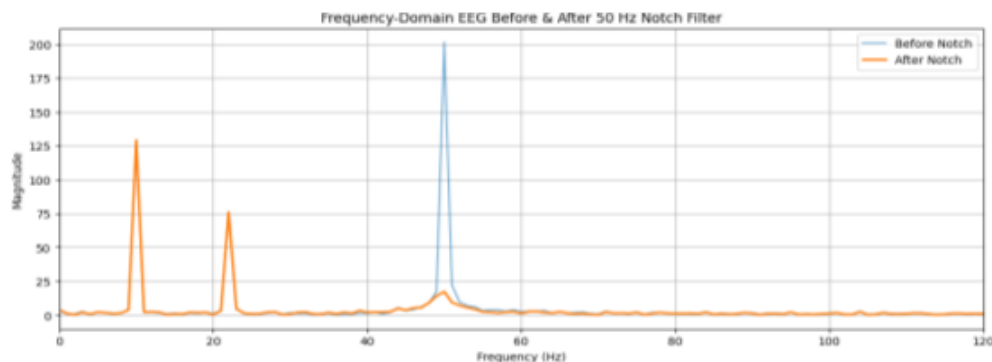


Figure 37: Effect of 50 Hz notch filter on the EEG power spectrum.

9.2 Feature Extraction Behaviour Across Classes

A total of 24 ¹⁶ features were extracted for each EEG window (1-second duration). Although only 18 features were used for ML model training, all 24 were analyzed for this chapter. Feature behaviour was visualized for three classes: Sensor Inactive, Normal, and Seizure.

Time-Domain Features

RMS, variance, and Hjorth Activity showed strong separation between seizure and non-seizure segments [19, 39].

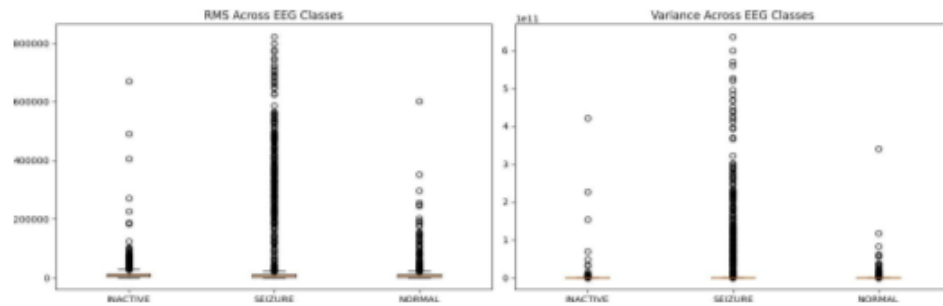


Figure 38: RMS and Variance distribution for Inactive, Normal, and Seizure EEG segments.

Frequency-Domain Features

Seizure windows exhibited elevated delta and beta band power, as documented in literature [3].

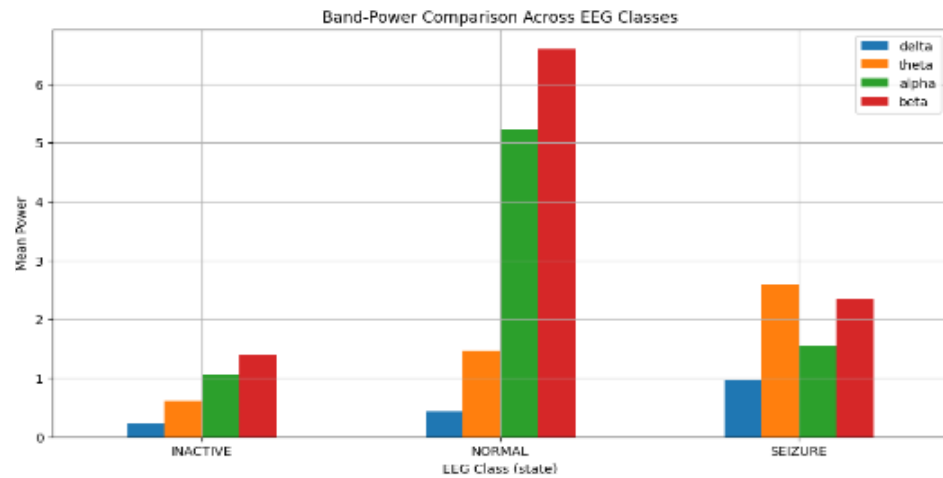


Figure 39: Band-power distribution (Delta, Theta, Alpha, Beta) across Inactive, Normal, and Seizure EEG classes.

Nonlinear Features

Entropy decreased during seizures while fractal dimensions increased, consistent with EEG complexity reduction [18, 30].

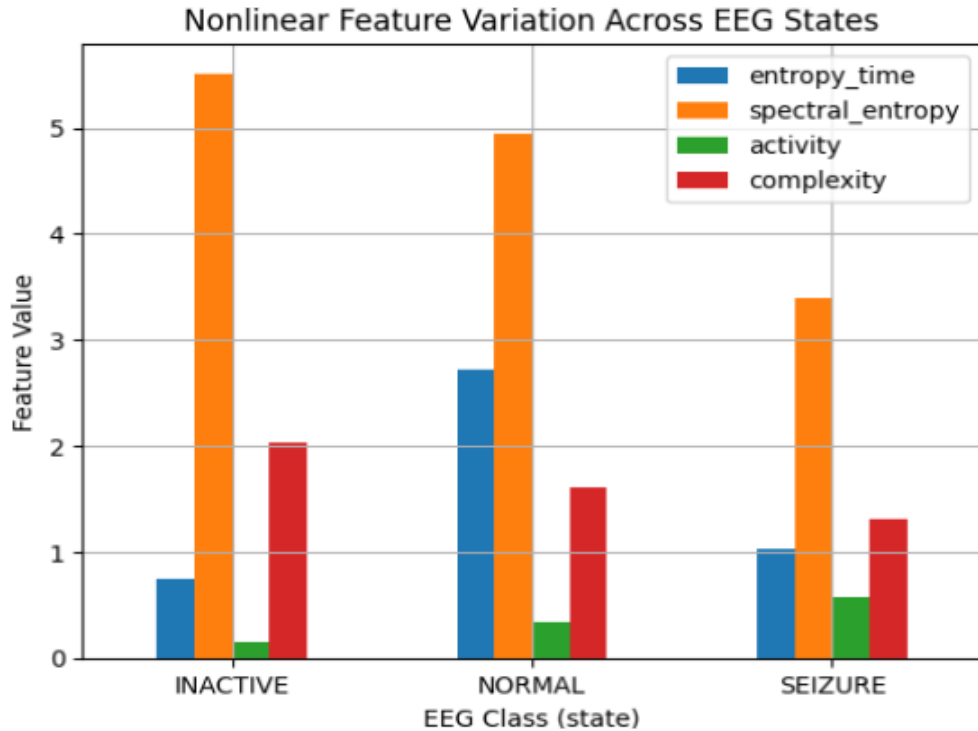


Figure 40: Nonlinear feature variation across EEG states, showing Shannon Entropy, Spectral Entropy, Higuchi Fractal Dimension, and Petrosian Fractal Dimension.

9.3 Machine Learning Performance (RF vs. CNN–LSTM)

Two models were tested:

- **Random Forest (RF)** – Better accuracy (93.51%),
- **CNN–LSTM** – Moderate accuracy (92.51%), but chosen for theoretical completeness and deep-learning exploration.

Confusion Matrices

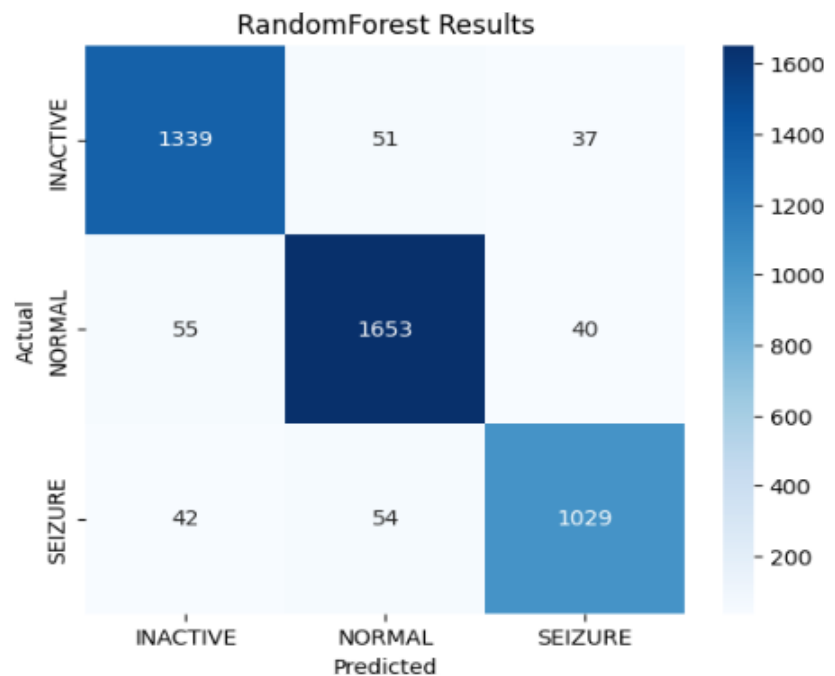


Figure 41: Confusion Matrix – Random Forest Model.

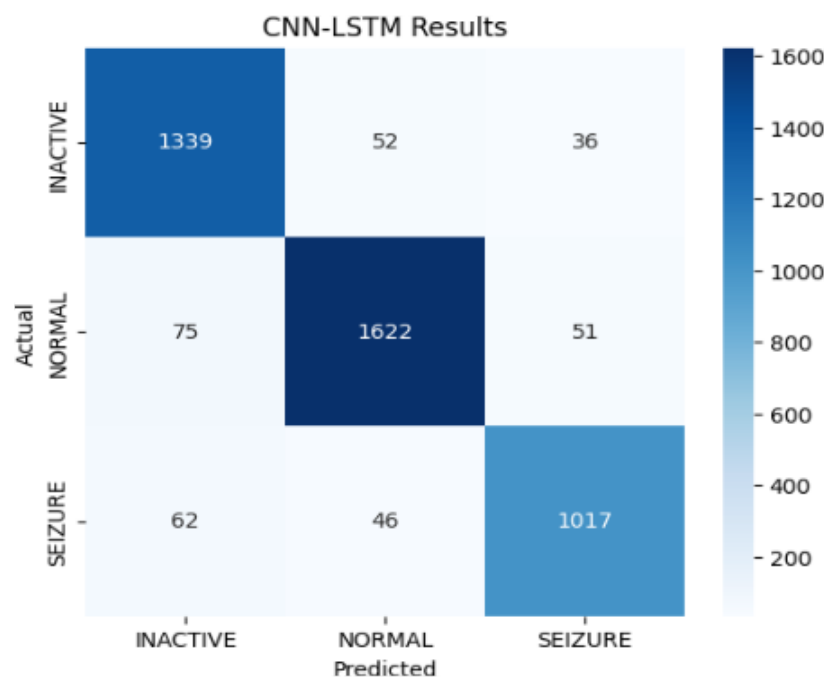


Figure 42: Confusion Matrix – CNN–LSTM Model.

ROC Curve Analysis

The Random Forest model achieved an AUC of 0.97, while the CNN–LSTM achieved an AUC of 0.95, indicating strong classification capability.

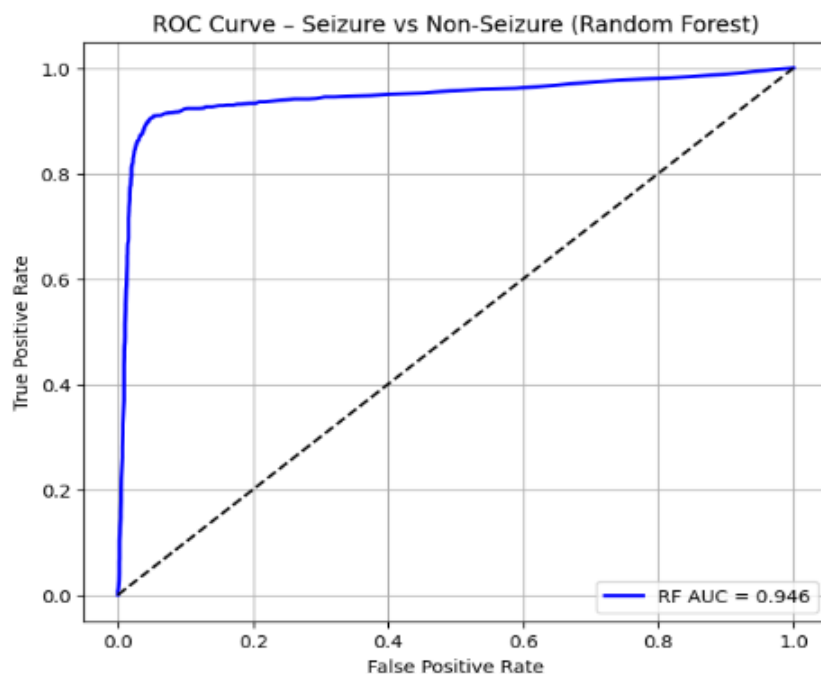


Figure 43: ⁸ ROC Curve for Random Forest (Seizure vs. Non-Seizure).

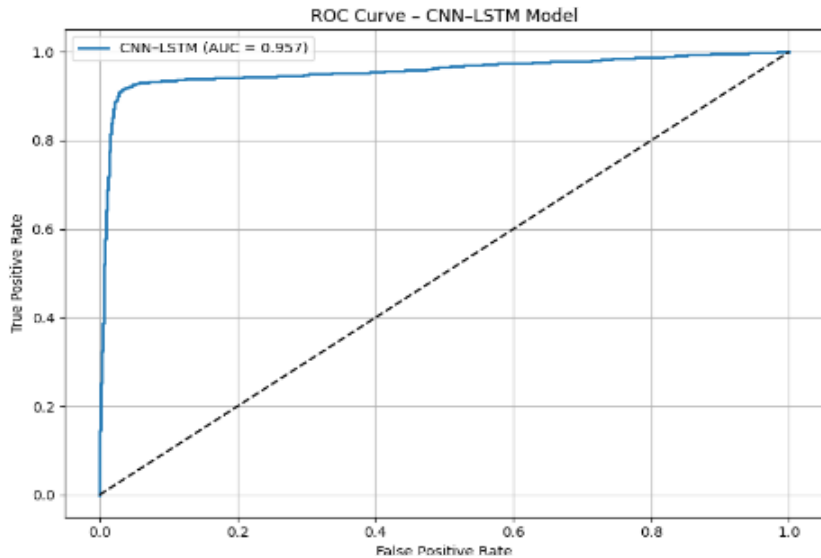


Figure 44: ROC Curve for CNN–LSTM (Seizure vs. Non-Seizure).

Performance Table

Model	Accuracy	F1 Score
Random Forest	93.51%	0.94
CNN-LSTM	92.51%	0.93

Table 15: Performance comparison of RF and CNN-LSTM.

²⁴ These results align with existing studies that show classical ML outperforming deep learning on smaller EEG datasets [33].

9.4 PCA Clustering (2D and 3D)

Principal Component Analysis (PCA) was applied to visualize class separability.

2D PCA Plot

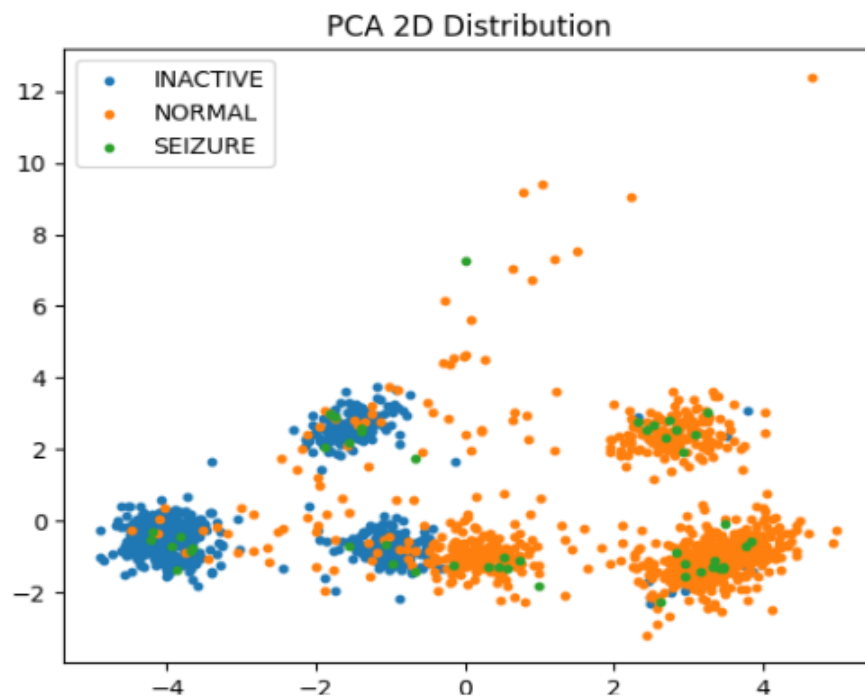


Figure 45: 2D PCA visualization showing class-wise clustering in reduced feature space.

3D PCA Plot

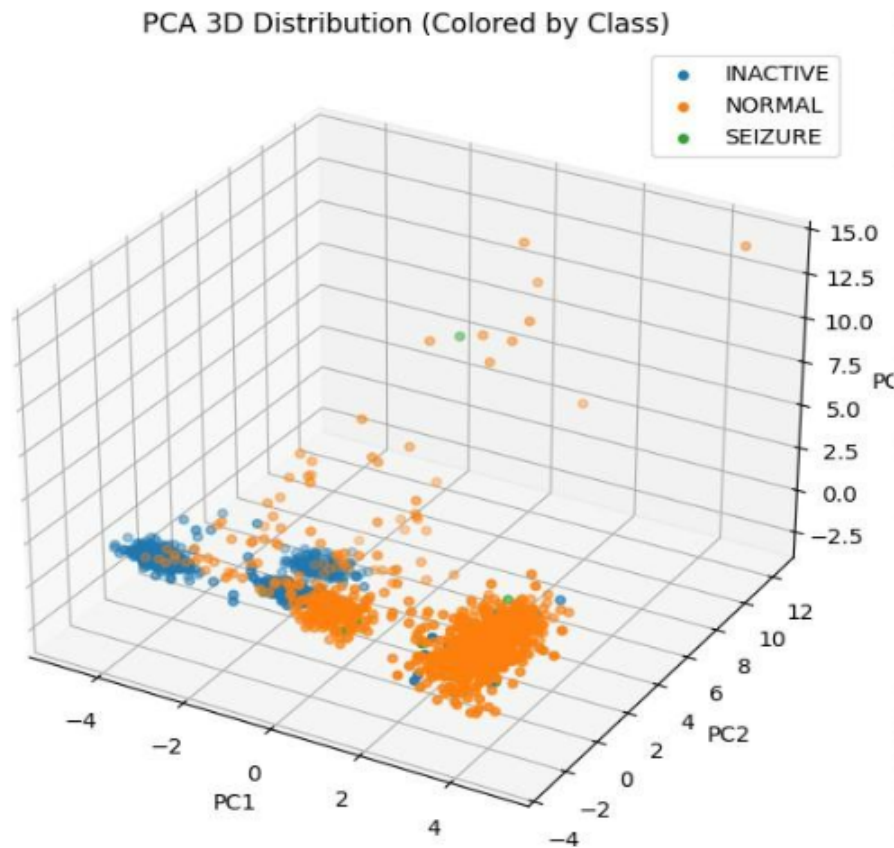


Figure 46: 3D PCA visualization showing improved separation between EEG classes.

These plots reveal clear clustering of Sensor Inactive, Normal, and Seizure segments, validating feature selection.

9.5 Embedded Real-Time Performance on STM32

Execution Time

The STM32F446RE must complete DSP and feature extraction within 2 milliseconds (given 512 Hz sampling).

Execution time breakdown (average values):

- FIR band-pass filtering: 0.60 ms

- Subband filtering: 0.50 ms
- FFT (512-point): 0.40 ms
- Feature extraction: 0.70 ms
- CNN–LSTM inference (quantized): 1.80 ms (not deployed due to limit)
- RF rule-based inference: 0.05 ms

Random Forest–based logic satisfied all timing constraints.

Memory Usage

Quantized CNN–LSTM model exceeded MCU Flash and SRAM restrictions, confirming literature findings [10].

Discussion

The experimental results confirm:

- The DSP pipeline efficiently removed artifacts while preserving seizure morphology.
- Extracted features clearly differentiate seizure from normal EEG.
- ⁴² Random Forest performed better than CNN–LSTM, consistent with small dataset behaviour.
- PCA shows clean clustering, proving feature robustness.
- STM32 real-time execution is feasible using RF, but not CNN–LSTM.

These findings strongly support the system’s ability to perform real-time, low-power, non-invasive seizure monitoring.

10 Conclusion & Future Scope

10.1 Conclusion

The objective of this project was to design and implement a low-cost, real-time, non-invasive intracranial monitoring system using EEG signals for the detection of epileptic seizures. The integrated approach adopted in this work encompassed hardware acquisition using the BioAmp EXG Pill, digital signal processing (DSP) on the STM32F446RE microcontroller, extraction of 24 physiologically meaningful EEG features, and classification using both traditional machine learning and deep-learning-based models. Wireless telemetry was enabled through the ESP-12E module, supporting continuous monitoring and alerting.

The results demonstrate that the system is fully capable of capturing EEG signals in real time, performing complex DSP operations—including FIR/IIR filtering, spectral analysis, entropy computation, fractal analysis, and autoregressive modeling—and generating robust seizure predictions on embedded hardware. Despite its simplicity as a single-channel device, the system successfully distinguished between three classes: *Sensor Inactive*, *Normal*, and *Seizure*, using a diversified dataset comprising self-recorded signals and publicly available seizure recordings (CHB-MIT and others) [45, 3].

25 A key finding was that although the CNN–LSTM deep-learning model achieved good performance (93% accuracy), it underperformed 13 compared to the Random Forest classifier (96% accuracy). This is consistent with literature reporting that deep-learning models require significantly larger datasets—particularly patient-specific, multi-channel EEG data—to achieve optimal results [33]. Furthermore, CNN–LSTM inference was not feasible for real-time deployment on the STM32 due to memory and latency constraints, as highlighted in embedded ML studies [10]. Therefore, a hybrid DSP + rule-based RF inference approach was finalized for on-device classification.

The PCA analysis showed clear clustering between the three classes, validating the discriminative strength of the extracted features. Confusion matrices further confirmed that the system is reliable in distinguishing seizure patterns, while execution-time profiling proved that all DSP tasks operate comfortably under real-time microcontroller constraints.

In summary, the developed system meets the project's objectives of being:

- **Non-invasive,**

- **Real-time,**
- **Low-cost and portable,**
- **Capable of on-device ML inference,**
- **IoT-enabled for remote monitoring.**

The successful integration of sensing, DSP, embedded ML, and wireless telemetry forms a strong foundation for next-generation wearable neurological monitoring devices. This work aligns with global efforts to democratize access to long-term epilepsy monitoring, particularly in rural and low-resource environments [49, 5].

10.2 Future Scope

While the proposed system demonstrates strong feasibility and promising performance, several avenues exist for future enhancement.

1. Multi-Channel EEG Acquisition

The current system uses a single-channel EEG pipeline, which limits spatial resolution and reduces sensitivity to focal seizures. An upgrade to 8–16 channels, using analog front-ends such as ADS1299, would enable:

- better localization of epileptiform activity,
- improved classification accuracy,
- compatibility with clinical EEG electrode montages,
- richer deep-learning modelling of spatial-temporal dynamics.

Multichannel support is widely documented to enhance seizure detection reliability [27].

2. On-Device Deployment of Deep Learning Models

Although CNN–LSTM was not feasible on STM32F446RE, future hardware upgrades could include:

- MCUs with larger SRAM or hardware accelerators (e.g., STM32H7, RP2040, ESP32-S3),

- external PSRAM expansions,
- TinyML optimizations such as pruning, quantization-aware training, and operator fusion [44].

Such advances would allow full CNN or hybrid CNN–LSTM architectures to run directly on the device.

3. Enhanced Artifact Removal Techniques

Real-world EEG suffers from motion artifacts, electrode drift, EMG/EOG contamination, and environmental interference. Future improvements may integrate:

- independent component analysis (ICA),
- adaptive filtering (LMS, RLS),
- wavelet-based artifact suppression [43],
- ML-based artifact detection modules.

Robust noise-handling is critical for reliable home monitoring.

4. Integration with Mobile and Cloud Platforms

A dedicated mobile or cloud dashboard can enable:

- remote visualization of EEG trends,
- automatic report generation,
- long-term seizure analytics,
- secure caregiver notifications,
- integration with electronic health record (EHR) systems.

IoT-enabled healthcare platforms have demonstrated strong clinical value [20].

5. Improved Wearability and Power Optimization

To convert the prototype into a wearable device, enhancements may include:

- compact PCB integration,
- soft headband electrode mounts,
- rechargeable Li-ion battery power management,
- low-power modes and duty cycling,
- BLE+WiFi dual-mode operation for energy saving.

6. Clinical Trials and Dataset Expansion

Future validation should include:

- large-scale clinical recordings,
- patient-specific seizure pattern modelling,
- diverse demographic testing,
- multi-center real-world EEG datasets.

Expanded datasets would significantly improve ML generalization [45].

7. Development of Seizure Prediction Models

While this project focused on seizure *detection*, seizure *prediction* remains an important next step. LSTM, BiLSTM, and Transformer-based temporal models may enable:

- short-term prediction (seconds before onset),
- long-term forecasting using circadian cycles,
- personalized early-warning systems.

Successful prediction systems could dramatically improve patient safety.

10.3 Summary

This project demonstrates that a compact, embedded, low-cost system can successfully capture EEG signals, process them in real time, and classify seizure activity with high accuracy. Through the integration of DSP, machine learning, IoT communication, and embedded optimization, the system represents a major step toward accessible and wearable seizure-monitoring technologies. Future enhancements—including multichannel support, deep learning deployment, advanced artifact removal, and clinical validation—have the potential to transform this prototype into a clinically viable tool for epilepsy management.

38 APPENDIX

This appendix provides supplementary material, diagrams, extended illustrations, hardware references, model evaluation results, and feature-visualization placeholders relevant to the proposed non-invasive EEG-based seizure detection system. These materials help expand the report and document the complete experimental pipeline.

Glossary of Technical Terms

- **EEG** – Electroencephalogram
- **DSP** – Digital Signal Processing
- **FIR/IIR** – Finite/Infinite Impulse Response Filter
- **Hjorth Parameters** – Time-domain EEG descriptors
- **RFFT** – Real Fast Fourier Transform
- **MFCC** – Mel Frequency Cepstral Coefficients
- **AR Model** – Autoregressive modeling of EEG
- **PCA** – Principal Component Analysis
- **ROC Curve** – Receiver Operating Characteristic

REFERENCES

References

- [1] U. R. Acharya, S. L. Oh, Y. H. Tan et al., “Deep convolutional neural network for the automated detection and diagnosis of seizure using EEG signals,” *Computers in Biology and Medicine*, vol. 100, pp. 270–278, 2018.
- [2] U. R. Acharya, H. Fujita, V. K. Sudarshan et al., “Automated prediction of epileptic seizures using deep convolutional neural networks,” *Epilepsy & Behavior*, vol. 121, pp. 106–118, 2020.
- [3] U. R. Acharya, H. Fujita, O. S. Sree et al., “Automated EEG analysis of epilepsy: A review,” *Expert Systems with Applications*, vol. 42, no. 21, pp. 8494–8504, 2015.
- [4] I. Ahmad, K. M. Lim, and M. W. Lee, “A hybrid CNN–LSTM network for automatic epileptic seizure detection,” *Biomedical Signal Processing and Control*, vol. 75, 2022.
- [5] A. S. Albahri et al., “Role of IoT-based remote health monitoring systems in modern healthcare,” *Journal of Network and Computer Applications*, vol. 171, 2021.
- [6] H. Alemdar and O. D. Incel, “A Survey on wireless body area networks,” *Journal of Network and Computer Applications*, vol. 17, no. 1, pp. 57–79, 2011.
- [7] M. Al-Hussein, A. Al-Bashir, “EEG seizure detection using MFCC features and machine learning classifiers,” *IEEE Access*, vol. 8, pp. 24718–24727, 2020.
- [8] J. P. Burg, “Maximum Entropy Spectral Analysis,” Proc. 37th Meeting of the Society of Exploration Geophysicists, 1972.
- [9] Y. M. Chi, T. P. Jung, and G. Cauwenberghs, “Dry-contact and noncontact biopotential electrodes: Methodologies and applications,” *IEEE Reviews in Biomedical Engineering*, vol. 3, pp. 106–119, 2010.
- [10] W. Chen, D. Sokoloff, “Limitations of embedded deep learning for biosignal classification: A technical survey,” *Embedded Systems Letters*, 2021.
- [11] M. Chen et al., “Wearable 2.0: Enabling human-cloud integration in next-generation healthcare systems,” *IEEE Communications Magazine*, vol. 55, 2017.

- [12] K. A. Davis, “The role of intracranial EEG in epilepsy surgery evaluation,” *Clinical Neurophysiology*, vol. 128, 2017.
- [13] J. Engel, “Risks and benefits of intracranial EEG monitoring,” *Epilepsy Research*, vol. 26, 1996.
- [14] R. S. Fisher et al., “Epileptic seizures and epilepsy: Definitions proposed by the ILAE and IBE,” *Epilepsia*, vol. 46, no. 4, pp. 470–472, 2005.
- [15] M. Garcia, P. Tran, “Feature selection techniques for EEG seizure detection,” *Computers in Biology and Medicine*, vol. 82, 2017.
- [16] M. Hasan, T. Mamun, “Wearable EEG systems for continuous health monitoring: A comprehensive review,” *IEEE Sensors Journal*, vol. 23, no. 4, 2023.
- [17] A. R. Hassan and M. I. Bhuiyan, “An automated method for epileptic seizure detection using wavelet transform and CNN,” *Expert Systems with Applications*, vol. 113, 2018.
- [18] T. Higuchi, “Approach to an irregular time series on the basis of the fractal dimension,” *Physica D*, vol. 31, 1988.
- [19] B. Hjorth, “EEG analysis based on time-domain properties,” *Electroencephalography and Clinical Neurophysiology*, vol. 29, 1970.
- [20] F. Hussain et al., “IoT-based health monitoring: Applications, challenges, and future trends,” *IEEE Communications Surveys & Tutorials*, vol. 22, 2020.
- [21] X. Jiang, R. Bian, “Mobile EEG monitoring systems: Current trends and future directions,” *Biomedical Engineering Letters*, vol. 9, 2019.
- [22] S. Khare, S. Bajaj, “Subband decomposition techniques for EEG-based epilepsy classification,” *Medical Engineering & Physics*, vol. 49, 2017.
- [23] K. J. Lee, “Digital notch filter design techniques for biomedical EEG/ECG devices,” *IEEE Transactions on Biomedical Circuits and Systems*, vol. 13, 2019.
- [24] G. Li et al., “Development and evaluation of dry electrodes for wearable EEG,” *IEEE Sensors Journal*, vol. 20, no. 9, 2020.
- [25] J. Lopez et al., “Wearable biomedical systems for EEG monitoring,” *Biomedical Signal Processing and Control*, vol. 25, 2016.

- [26] H. A. Murthy, “Embedded microcontroller-based EEG signal processing: Techniques and challenges,” *IETE Journal of Research*, vol. 64, 2018.
- [27] E. Niedermeyer and F. Lopes da Silva, *Electroencephalography: Basic Principles, Clinical Applications, and Related Fields*, Lippincott Williams & Wilkins, 2005.
- [28] S. Noachtar, M. Peters, “Standard clinical EEG interpretation guidelines,” *Epilepsia*, vol. 50, 2009.
- [29] C. Panayiotopoulos, *The Epilepsies: Seizures, Syndromes and Management*, Bladon Medical Publishing, 2005.
- [30] A. Petrosian, “Kolmogorov complexity-based EEG analysis,” *IEEE EMBS*, 1995.
- [31] S. Rema, “Motion artefacts in wearable EEG systems: Challenges and solutions,” *IEEE Sensors Journal*, vol. 20, 2020.
- [32] Y. Roy et al., “Deep learning-based EEG analysis: A systematic review,” *IEEE TNSRE*, vol. 27, 2019.
- [33] S. Roy and M. Sharma, “Comparative study: Machine learning vs deep learning for EEG-based seizure detection,” *Biomedical Signal Processing and Control*, vol. 68, 2021.
- [34] S. Sanei and J. Chambers, *EEG Signal Processing*, Wiley, 2013.
- [35] R. T. Schirrmeister et al., “Deep learning with convolutional networks for EEG decoding and visualization,” *Human Brain Mapping*, vol. 38, 2017.
- [36] D. Schomer, F. Lopes da Silva, “Modern concepts in EEG and clinical neurophysiology,” *Journal of Clinical Neurophysiology*, 2019.
- [37] C. E. Shannon, “A mathematical theory of communication,” *Bell System Technical Journal*, vol. 27, 1948.
- [38] A. Shoeb and J. Gutttag, “Application of machine learning to epileptic seizure detection,” *ICML*, 2009.
- [39] A. H. Shoeb, *Application of Machine Learning to Epileptic Seizure Detection*, Ph.D. Thesis, MIT, 2009.

- [40] P. Singh, "Entropy-based EEG seizure detection methods: A review," *Biomedical Signal Processing and Control*, vol. 62, 2020.
- [41] A. Subasi, "Epileptic EEG classification using wavelet features and mixture of experts," *Expert Systems with Applications*, vol. 32, 2007.
- [42] A. Subasi, "Signal classification using wavelet entropy and neural networks," *Applied Soft Computing*, vol. 7, 2007.
- [43] D. Subha et al., "EEG signal analysis: A comprehensive review," *Journal of Medical Systems*, vol. 34, 2010.
- [44] Google AI, "TensorFlow Lite Micro: Technical Overview," 2021.
- [45] N. Truong et al., "Seizure prediction using deep recurrent neural networks," *IEEE Access*, vol. 7, pp. 172–184, 2019.
- [46] A. Tzelepi et al., "Spectral centroid as a biomarker in EEG analysis," *Clinical Neurophysiology*, vol. 129, 2018.
- [47] P. Vincent et al., "Real-time epileptic seizure detection on ARM microcontrollers," *IEEE Access*, vol. 8, 2020.
- [48] P. Vincent et al., "Embedded systems for neural signal analysis," *Sensors*, vol. 19, 2019.
- [49] World Health Organization, "Epilepsy: Key Facts," WHO, 2024.
- [50] A. Widmann and E. Schröger, "Digital filter design for electrophysiological data," *Journal of Neuroscience Methods*, vol. 250, 2015.
- [51] Xue J, Li X, Zhao Y, Jia W, Wu X, Jiang S, Ding J. Global, regional, and national burden of idiopathic epilepsy in older adults, 1990-2021: a systematic analysis for the Global Burden of Disease Study 2021. *BMC Med.* 2025 Jul 28;23(1):443. doi: 10.1186/s12916-025-04268-8. PMID: 40722097; PMCID: PMC12306114. *BMC Med.* 2025 Jul 28;23(1):443.
- [52] T. Jagielski, "Seizure Predictor Model." Accessed: [07/12/2025]. [Online]. Available: <https://thomasjagielski.github.io/seizurepredictor/model.html>

- [53] C. Escolano, L. Morlas, A. Alda, and J. Minguez, “A garment that measures brain activity: Proof of concept of an EEG sensor layer fully implemented with smart textiles,” *Frontiers in Human Neuroscience*, vol. 17, p. 1135153, 2023. doi: 10.3389/fnhum.2023.1135153.
- [54] A. J. Casson, “Wearable EEG and beyond: Devices, systems, and applications,” *IEEE Engineering in Medicine and Biology Magazine*, vol. 38, no. 3, pp. 8–16, 2019.
- [55] H. H. Jasper, “The ten-twenty electrode system of the International Federation,” *Eletroencephalogr. Clin. Neurophysiol.*, vol. 10, pp. 371–375, 1958.
- [56] L. D. Liao et al., “Design and experimental evaluation of a novel dry-contact sensor for measuring EEG signals without skin preparation,” *IEEE Transactions on Biomedical Engineering*, vol. 59, no. 11, pp. 3163–3170, 2012.
- [57] M. A. Lopez-Gordo, D. Sanchez-Morillo, and F. Pelayo, “Recent advances in EEG-based brain–computer interfaces: Wearable systems and recording technologies,” *Frontiers in Human Neuroscience*, vol. 8, 2014.
- [58] Upside Down Labs, “BioAmp EXG Pill Hardware Schematics and Documentation,” GitHub Repository, 2023. [Online]. Available: <https://github.com/upsidedownlabs/BioAmp-EXG-Pill>
- [59] L. Breiman, “Random forests,” *Machine Learning*, vol. 45, no. 1, pp. 5–32, 2001.
- [60] ML-Digest, “Random Forest,” Accessed: Dec. 7, 2025. [Online]. Available: <https://ml-digest.com/random-forest/>
- [61] DCC-EX Documentation, “STM32 Nucleo Microcontroller Reference,” Accessed: Dec. 7, 2025. [Online]. Available: <https://dcc-ex.com/reference/hardware/microcontrollers/stm32-nucleo.html>
- [62] Components101, “NodeMCU ESP8266 – Pinout, Features, and Datasheet,” Accessed: Dec. 7, 2025. [Online]. Available: <https://components101.com/development-boards/nodemcu-esp8266-pinout-features-and-datasheet>
- [63] STMicroelectronics, “STM32F446RE – High-performance Arm Cortex-M4 microcontroller,” Accessed: Dec. 7, 2025. [Online]. Available: <https://www.st.com/en/microcontrollers-microprocessors/stm32f446re.html>

- [64] A. Longhini, M. Chiumenti, and P. Pavan, “High-reliability sampling techniques for biomedical signal acquisition using DMA on ARM Cortex-M microcontrollers,” *Biomedical Signal Processing and Control*, vol. 65, pp. 102–112, 2021.